Article

Molecular Cell

Imprinted Maternally Expressed microRNAs Antagonize Paternally Driven Gene Programs in Neurons

Graphical Abstract

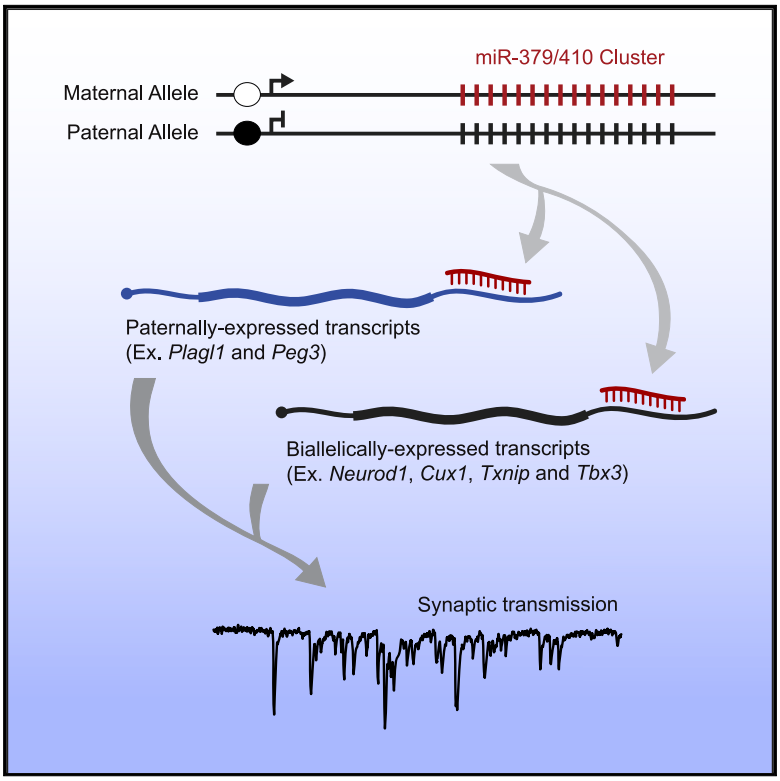

Highlights

- Neuron differentiation of hybrid ESCs can be used to study imprinted gene activity
- A miRNA cluster is expressed from the maternally inherited allele in induced neurons
- Maternally expressed miR-379/410 targets paternally expressed transcripts
- miR-379/410 also regulates genes involved in synaptic activity and neuron function

Authors

Amanda J. Whipple, Vincent Breton-Provencher, Hannah N. Jacobs, Udbhav K. Chitta, Mriganka Sur, Phillip A. Sharp

Correspondence

amanda_whipple@fas.harvard.edu (A.J.W.), sharppa@mit.edu (P.A.S.)

In Brief

Some miRNAs are regulated by genomic imprinting, but the evolutionary benefits and consequences of parental-biased miRNA expression are unknown. Whipple et al. show that maternally expressed miRNAs target transcriptional and developmental regulators, including paternally expressed transcripts, suggesting these miRNAs may increase matrilineal inclusive fitness by antagonizing paternally driven gene programs.

Whipple et al., 2020, Molecular Cell *78*, 1–11
April 2, 2020 Published by Elsevier Inc.
https://doi.org/10.1016/j.molcel.2020.01.020

CellPress

Please cite this article in press as: Whipple et al., Imprinted Maternally Expressed microRNAs Antagonize Paternally Driven Gene Programs in Neurons, Molecular Cell (2020), https://doi.org/10.1016/j.molcel.2020.01.020

Molecular Cell
Article

Imprinted Maternally Expressed microRNAs Antagonize Paternally Driven Gene Programs in Neurons

Amanda J. Whipple,[1,2,5,*] Vincent Breton-Provencher,[3] Hannah N. Jacobs,[4] Udbhav K. Chitta,[2] Mriganka Sur,[3] and Phillip A. Sharp[1,*]

[1]Koch Institute for Integrative Cancer Research, Massachusetts Institute of Technology, Cambridge, MA 02139, USA
[2]Department of Molecular and Cellular Biology, Harvard University, Cambridge, MA 02138, USA
[3]Picower Institute for Learning and Memory, Department of Brain and Cognitive Sciences, Massachusetts Institute of Technology, Cambridge, MA 02139, USA
[4]Biological Sciences Department, Wellesley College, Wellesley, MA 02481, USA
[5]Lead Contact
*Correspondence: amanda_whipple@fas.harvard.edu (A.J.W.), sharppa@mit.edu (P.A.S.)
https://doi.org/10.1016/j.molcel.2020.01.020

SUMMARY

Imprinted genes with parental-biased allelic expression are frequently co-regulated and enriched in common biological pathways. Here, we functionally characterize a large cluster of microRNAs (miRNAs) expressed from the maternally inherited allele ("maternally expressed") to explore the molecular and cellular consequences of imprinted miRNA activity. Using an induced neuron (iN) culture system, we show that maternally expressed miRNAs from the miR-379/410 cluster direct the RNA-induced silencing complex (RISC) to transcriptional and developmental regulators, including paternally expressed transcripts like *Plagl1*. Maternal deletion of this imprinted miRNA cluster resulted in increased protein levels of several targets and upregulation of a broader transcriptional program regulating synaptic transmission and neuronal function. A subset of the transcriptional changes resulting from miR-379/410 deletion can be attributed to de-repression of Plagl1. These data suggest maternally expressed miRNAs antagonize paternally driven gene programs in neurons.

INTRODUCTION

Genomic imprinting is an epigenetic phenomenon that results in preferential gene expression from the maternally or paternally inherited allele (hereafter "maternally expressed" or "paternally expressed"). Imprinting impacts disease predisposition by negating the ability of diploid organisms to buffer against recessive mutations, and the evolutionary pressures driving imprinting are openly debated (Haig, 2014; Patten et al., 2014; Spencer and Clark, 2014). Nevertheless, interaction among imprinted genes is predicted by evolutionary theories and supported by experimental findings. Many imprinted genes are functionally related and found in common biological pathways, such as those regulating nutrient control and growth (Peters, 2014). Studies in mice have shown that opposing parental alleles differentially affect growth pathways whereby paternally expressed genes enhance growth and maternally expressed genes repress growth. Imprinted genes are frequently co-regulated and may be members of a common gene network coordinated by *cis*-acting and *trans*-acting factors (Al Adhami et al., 2015; Patten et al., 2016; Varrault et al., 2006). The mechanisms by which such an imprinted gene network may be coordinately regulated is not apparent.

Many microRNAs (miRNAs) have evolved imprinted expression, but the potential evolutionary benefits and consequences of parental-biased miRNA expression remain to be determined. miRNAs direct post-transcriptional repression of mRNA targets through the RNA-induced silencing complex (RISC). There are three recently evolved, imprinted miRNA clusters. miRNA clusters in the rodent-specific *Sfmbt2* and primate-specific *C19MC* genes are paternally expressed in the placenta (Noguer-Dance et al., 2010; Wang et al., 2011), whereas the eutherian-specific *Maternally expressed gene 3* (*Meg3)* miRNA clusters are maternally expressed in multiple tissues including the brain (Seitz et al., 2003). While miRNAs typically exert modest effects on gene expression, the physiological effects of miRNA clusters may be amplified by coordinated co-expression of multiple miRNAs and co-targeting of multiple mRNAs in a biological pathway. Interestingly, a key RISC component, *Argonaute2* (*Ago2)*, also exhibits maternally biased expression in the brain (Andergassen et al., 2017; Bonthuis et al., 2015; Perez et al., 2015), suggesting the maternal genome may benefit from miRNA activity in the brain. Therefore, we sought to characterize the potential impact of maternally expressed miRNAs in neurons.

A dense cluster of 39 miRNAs, miR-379/410, is located in the terminal region of *Meg3* known as *Mirg* (Figure 1A). The miR-379/410 cluster is expressed during early development and in postnatal brain (Labialle et al., 2014). Maternal inheritance of miR-379/410 deletion in mice resulted in hypoglycemia immediately after birth (Labialle et al., 2014), suggesting these miRNAs control metabolic physiology during early development. Adult mice with maternal miR-379/410 deletion display anxiety-related behaviors and increased sociability, perhaps due to alterations in synaptic signaling (Lackinger et al., 2019; Marty et al., 2016). One

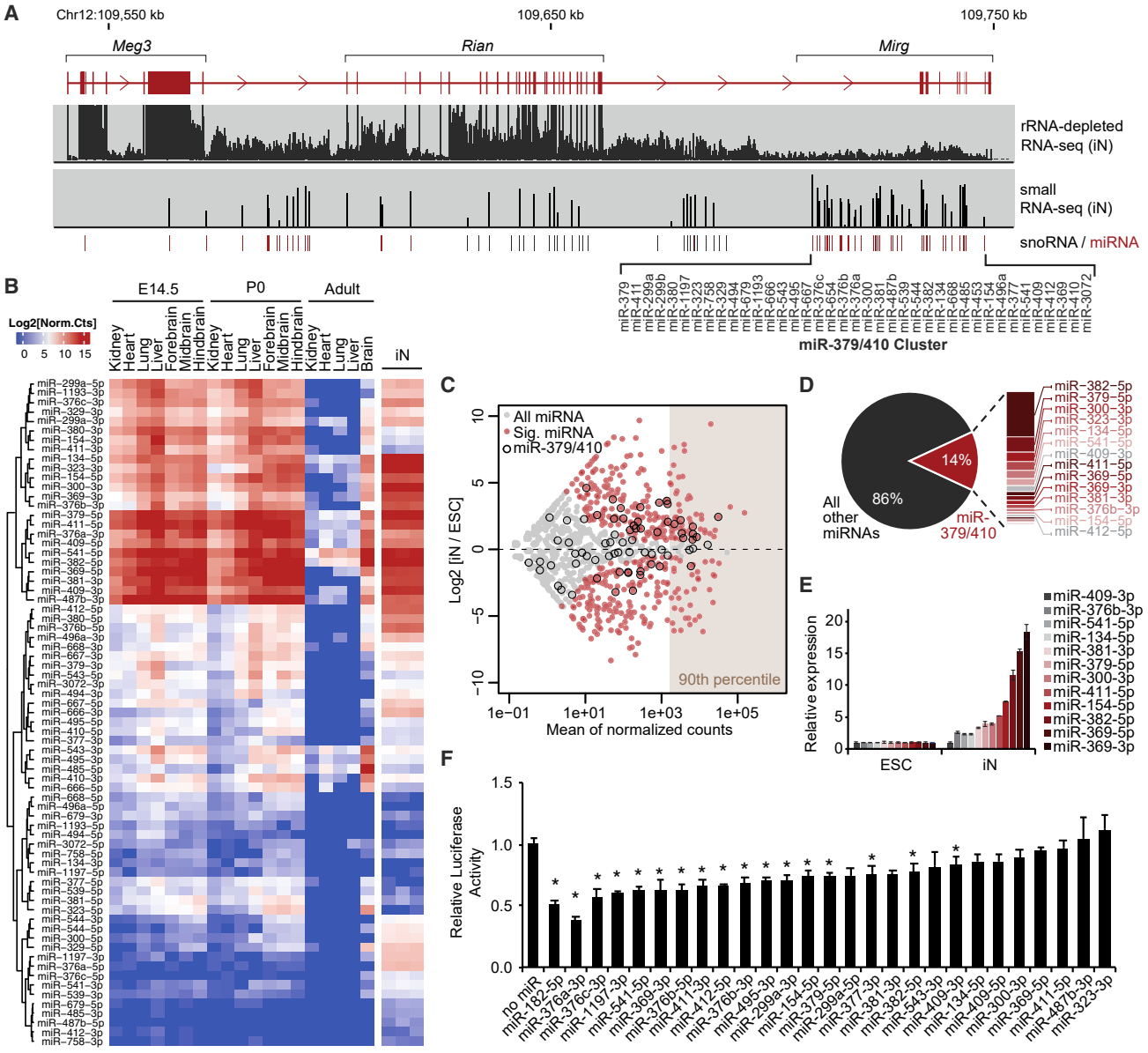

Figure 1. miR-379/410 Expression Is Induced upon Neuron Differentiation

(A) Schematic of the annotated *Meg3* long non-coding RNA and small non-coding RNAs processed from the locus (snoRNA, small nucleolar RNA; miRNA). The location of the miR-379/410 cluster is indicated, along with genomic alignment of rRNA-depleted RNA-seq and small RNA-seq data from iNs.

(B) Heatmap of normalized counts of mature miRNAs from the miR-379/410 cluster generated by small RNA-seq of mouse tissues at embryonic day 14.5 (E14.5), postnatal day 0 (P0), adult tissues, and *in vitro* differentiated iNs (n = 3). Rows are organized by unsupervised hierarchical clustering.

(C) Expression changes of miRNAs upon neuron differentiation shown as an MA plot. Gray, all miRNAs; red, differentially expressed miRNAs ($p \leq 0.05$, fold change ≥ 2); black outline, miR-379/410. miRNAs in the 90th percentile of expression are indicated.

(D) Pie chart indicating the proportion of small RNA-seq reads mapping to miR-379/410 miRNAs versus all other miRNAs in iNs.

(E) qRT-PCR for mature miRNAs from miR-379/410 in iNs relative to ESCs. Mean ± SEM (n = 3).

(F) Bar graph of Firefly luciferase activity with or without 3′ UTR miRNA target sites relative to Renilla luciferase internal control. Mean ± SEM (n = 6); *$p \leq 0.05$, calculated using unpaired two-tailed Student's t test. See also Figure S1.

miRNA from the cluster, miR-134-5p, localizes to the synapse and regulates dendritic spine size through translational repression of *Limk1* and *Pum2* (Fiore et al., 2009; Schratt et al., 2006). However, relatively few targets of this large miRNA cluster have been identified, and molecular understanding of how these miRNAs may coordinately regulate biological processes is lacking.

In this study, we sought to understand the molecular and cellular consequences of imprinted miRNA activity by performing a comprehensive characterization of miR-379/410 targets

in neurons. We generated a powerful discovery model for imprinted miRNA activity using Neurogenin2-induced differentiation of hybrid mouse embryonic stem cells (ESCs) to induced neurons (iNs). Using this system, we identified 33 active miRNAs from the imprinted miR-379/410 cluster. We found that these maternally expressed miRNAs direct the RISC machinery to paternally expressed transcripts, including *Plagl1* and *Peg3*, resulting in increased protein levels upon maternal miR-379/410 deletion. We also identified additional miR-379/410 targets that function in transcriptional and developmental regulation, like *Neurod1*. Moreover, we determined that neurons with maternal miR-379/410 deletion have aberrant upregulation of genes associated with synaptic processes, including downstream transcriptional targets of Plagl1 and NeuroD1. These data suggest the maternal genome utilizes the miRNA pathway to antagonistically regulate paternally driven gene programs in neurons.

RESULTS

miR-379/410 Expression Is Induced upon Neuron Differentiation

To determine the relative levels of mature miRNAs produced from the miR-379/410 cluster during development, we analyzed small RNA-seq data from mouse peripheral tissues and brain regions at embryonic, early postnatal, and adult developmental stages (Figure 1B). A distinct subgroup of 24 mature miRNAs located throughout the cluster are highly expressed across all embryonic and early postnatal tissues. These miRNAs are downregulated during postnatal development, resulting in little to no expression of miR-379/410 in adult tissues except brain, which maintains high expression in adulthood. Expression of the *Meg3*/*Mirg* host gene is also abundant in the brain (Figure S1A) and shows higher levels in neurons compared to astrocytes, microglia, or other brain-derived cell types (Figure S1B).

We established an *in vitro* neuron differentiation system to study the maternally expressed miR-379/410 cluster. Doxycycline-inducible *Neurogenin2* (*Ngn2*) was stably integrated into F1 hybrid mouse ESCs from a *Mus. musculus* x *Mus. castaneous* cross (Eggan et al., 2001) that allows maternal and paternal alleles to be distinguished by single nucleotide polymorphisms (SNPs) (Figure S1C). Upon differentiation by doxycycline treatment, iNs expressed markers of glutamatergic neurons and displayed spontaneous electrophysiological activity (Figure S1D–S1G). We performed small RNA-seq to determine the dynamics of miRNA expression upon neuron differentiation. We found that miR-379/410 expression in iNs mimics *in vivo* expression (Figure 1B). Many miRNAs from the cluster are among the most highly expressed miRNAs upon differentiation (Figure 1C). In fact, we found that 14% of all miRNAs detected in iNs were from the miR-379/410 cluster (Figure 1D). We confirmed upregulation of miR-379/410 in iNs by qRT-PCR and northern blot (Figures 1E and S1H). We conclude that a subset of the miR-379/410 cluster is highly expressed and dynamically regulated during development and differentiation.

We then asked if miR-379/410 showed repressive activity in iNs. Perfect target sites for individual miRNAs from the cluster were inserted into the 3′ UTR of a luciferase reporter, and luciferase activity was measured in iNs. We found sixteen miRNAs from the cluster significantly repressed luciferase activity by 10%–60% ($p \leq 0.05$) (Figure 1F). The perfect target site for miR-182-5p, an abundant miRNA in iNs, was used as a positive control and resulted in 50% repression of luciferase activity. These data indicate that Ngn2-induced neurons are a great system for identifying miR-379/410 targets.

Identification of RISC-Associated miRNAs in Induced Neurons

In order to determine which miRNAs and mRNA target sites are bound by the RISC complex in iNs, we performed Ago2 single-end enhanced crosslinking and immunoprecipitation (seCLIP-seq). We stably integrated a transgene expressing untagged-Ago2 or HA-Ago2 into ESCs, differentiated cells to iNs, and performed seCLIP-seq using HA antibody (Figure S2A). We identified 211 Ago2-bound miRNAs, including 27 miRNAs from the miR-379/410 cluster ($p \leq 0.01$, fold change ≥ 2) (Figures 2A and S2B). The miRNAs most highly bound by Ago2 were miR-300-3p, miR-541-5p, miR-485-3p, and miR-758-3p, a finding that was independently confirmed by RNA immunoprecipitation followed by qRT-PCR (Figure S2C). The expression, reporter activity, and Ago2 association of all mature miRNAs from the miR-379/410 cluster are summarized in Figure S2D. Based on these data, we sought to identify targets of active miR-379/410 miRNAs, which we defined as the 33 miRNAs with significant Ago2 binding or repressive reporter activity.

We called peaks in mapped seCLIP-seq reads that were significantly enriched in HA-Ago2 IP samples relative to untagged-Ago2 IP or input samples ($p \leq 0.01$, fold change ≥ 2). Seventy-five percent of the significantly enriched Ago2 peaks were located in mRNA 3′ UTRs (Figures 2B and S2E), consistent with known miRNA activity (Bartel, 2018). A subset of 3′ UTR peaks overlapped seed sites for active miRNAs from the miR-379/410 cluster. Before investigating miR-379/410 targets, we first analyzed the seed families represented in the cluster. The targeting properties of mature miRNAs are dictated by their seed sequence, a 7-nucleotide sequence that directs RISC to mRNA targets (Bartel, 2018). miRNAs with identical seed sequence are members of a seed family and potentially share mRNA target sites. We grouped the 78 mature miRNAs from the cluster into 70 distinct families based on their 7-mer seed sequences (Figure S2F). We found 60 seed families unique to miR-379/410 and 10 families that share a seed sequence with a miRNA outside the cluster. In the latter category, seed families with multiple expressed family members were excluded from subsequent analysis since repressive activity cannot be conclusively attributed to miR-379/410.

We independently analyzed evolutionarily conserved and nonconserved seed sites with significantly enriched Ago2 peaks and found that four miRNAs (miR-543-3p, miR-369-3p, miR-154-5p, and miR-495-3p) had the highest number of Ago2-bound conserved seed sites (Figure S2G). Similarly, in a metagene analysis for Ago2 abundance at miRNA seed sites, we observed an enrichment for Ago2 at conserved seed sites for these four miRNAs, but not at nonconserved seed sites (Figure 2C). A similar result was observed in metagene profiles for all active miR-379/410 miRNAs combined (Figure S2H). Using Ago2 seCLIP-seq, we identified miRNAs from the maternally

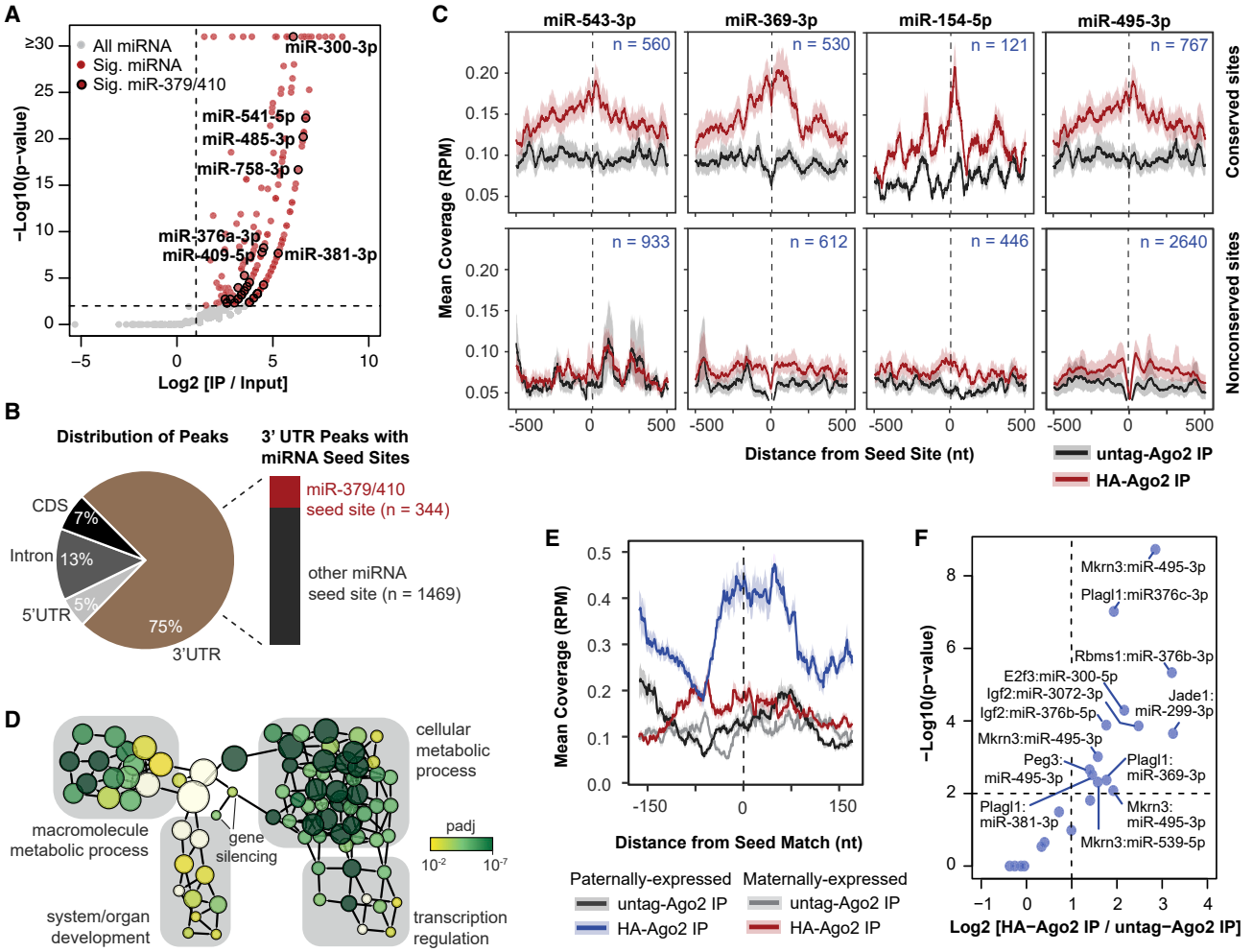

Figure 2. miR-379/410 Directs Ago2 to Transcriptional and Developmental Regulators, Including Paternally Expressed Transcripts

(A) Volcano plot of seCLIP-seq reads mapped to miRNAs. Gray, all miRNAs (n = 2,045); red, significantly enriched miRNAs ($p \leq 0.01$, fold change ≥ 2, n = 211); black outline, significantly enriched miR-379/410 ($p \leq 0.01$, fold change ≥ 2, n = 27). The identities of the most highly enriched miR-379/410 miRNAs are labeled.

(B) Left: Pie chart indicating distribution of significant Ago2 peaks in 5′ UTR, intron, CDS (coding sequence), and 3′ UTR. Right: Bar graph of the number of significant Ago2 peaks in 3′ UTRs that overlap with a seed site for an active miR-379/410 miRNA.

(C) Metagene plots of Ago2 seCLIP-seq coverage (reads per million, RPM) at seed sites for the indicated miRNAs, including coverage 500 nt upstream and downstream of the seed site. The number of sites included in each plot is shown. Top, conserved sites; bottom, nonconserved sites with TargetScan score ≥ 90; black, untagged-Ago2 IP; red, HA-Ago2 IP.

(D) Biological network of gene ontology terms associated with miR-379/410 targets identified by Ago2 seCLIP-seq. The node size corresponds to the number of genes in the node. The node color indicates the adjusted p value for the association of the gene ontology term with the miR-379/410 targets relative to the background of all expressed genes.

(E) Metagene plot of Ago2 seCLIP-seq coverage (reads per million, RPM) at conserved seed sites for active miR-379/410 in paternally expressed transcripts (n = 33 seed sites) and maternally expressed transcripts (n = 25 seed sites), including coverage 175 nt upstream and downstream of the seed site.

(F) Volcano plot of Ago2 peaks in paternally expressed transcripts. Dashed lines, cutoffs for significant peaks ($p \leq 0.01$, fold change ≥ 2). See also Figure S2 and Table S1.

expressed miR-379/410 cluster that are active in iNs and guide Ago2 to target sites on mRNAs.

miR-379/410 Directs Ago2 to Transcriptional and Developmental Regulators, Including Paternally Expressed Transcripts

Next, we examined the identity and functional classification of the 226 targets with significant Ago2 binding at miR-379/410 seed sites (Table S1). Ontology analysis of these miRNA targets indicated they are enriched for functions in transcription, development, and diverse metabolic processes (Figure 2D). The miR-379/410 targets include *Neurod1* and *Cux1*, transcription factors involved in neuron differentiation and development, as well as the synaptic vesicle glutamate transporter *Slc17a6*. We also observed miR-379/410 targets associated with central control of nutrient regulation, such as *Txnip* and *Tbx3*, which

are expressed in energy-sensing neurons and regulate feeding response (Blouet and Schwartz, 2011; Quarta et al., 2019).

Given the precedent for co-regulated expression of imprinted genes, we hypothesized that maternally expressed miRNAs may direct the RISC complex to imprinted transcripts. We analyzed metagene profiles of Ago2 abundance at miR-379/410 seed sites on transcripts known to be imprinted from previous *in vivo* studies. Ago2 was highly bound at miR-379/410 seed sites on paternally expressed transcripts, but not on maternally expressed transcripts (Figure 2E). In fact, the mean coverage of Ago2 binding at seed sites in paternally expressed transcripts was more than twice the coverage at seed sites in non-imprinted transcripts (Figure S2H). miR-379/410 targets were enriched for paternally expressed transcripts more than expected by chance ($p = 7 \times 10^{-5}$, hypergeometric test), and some of the paternally expressed transcripts were co-targeted by multiple miRNAs from the cluster (Figure 2F). *Plagl1* and *Peg3* are transcriptional drivers of paternal programs in the brain, impacting feeding behavior, energy homeostasis, growth, and neurogenesis (Abreu et al., 2013; Curley et al., 2005; Rraklli et al., 2016; Tanaka et al., 2019; Varrault et al., 2006). *Igf2* is a paternally expressed gene that controls embryonic growth (DeChiara et al., 1991; Ferguson-Smith et al., 1991), but whose function in the postnatal brain remains poorly defined. In fact, several reports indicate *Igf2* switches to maternal-biased expression in the brain (Andergassen et al., 2017; Bonthuis et al., 2015; Perez et al., 2015). Thus, it is possible miR-379/410 targeting of *Igf2* may have arisen from regulation in peripheral tissues during early development. Overall, these data suggest maternally expressed miR-379/410 acts to modulate transcriptional and developmental processes in iNs, partly by recruiting the RISC complex to paternally expressed transcripts.

miR-379/410 Targets Are De-repressed upon Maternal miR-379/410 Deletion

To determine the effect of miR-379/410 regulation on its targets, we generated cells with maternal-specific deletion of the entire 50-kb miRNA cluster. We co-transfected hybrid ESCs with dual single guide RNAs complementary to sites flanking the miR-379/410 host gene (“*Mirg*”) and loxP-containing donor oligonucleotides. We identified a $Mirg^{fl/+}$ clonal cell line with dual loxP insertion on the maternal allele by Sanger sequencing across allele-specific SNPs and subsequently deleted the intervening miRNA cluster by transient transfection of Cre recombinase (Figures 3A and S3A). Expression of *Mirg* was completely lost in $Mirg^{\Delta/+}$ cells, and no mature miRNAs from the miR-379/410 cluster were produced (Figures 3B, S3B, and S3C). $Mirg^{\Delta/+}$ ESCs exhibited no significant change in their rate of proliferation or differentiation (Figures S3D and S3E), and iN morphology appeared normal (Figure S3F). In $Mirg^{\Delta/+}$ iNs, we observed loss of miR-379/410 activity indicated by significant de-repression of luciferase reporters containing perfect miRNA target sites (Figure 3C).

We next analyzed the protein level of miR-379/410 targets in $Mirg^{fl/+}$ and $Mirg^{\Delta/+}$ cells. $Mirg^{\Delta/+}$ iNs had increased protein levels of NeuroD1 and Txnip. We also observed increased protein levels of the imprinted targets, Plagl1, Peg3, Jade1, and Igf2, upon maternal miR-379/410 deletion in iNs (Figure 3D). We confirmed a similar effect in a second subclonal cell line (Figure S4). In ESCs, the protein levels were unaffected or weakly increased, consistent with the induction of miR-379/410 upon differentiation. The mRNA levels of imprinted transcripts were unaffected by miR-379/410 deletion, suggesting the miRNA effect is not through mRNA destabilization (Figures S3G and S3H).

To test if *Plagl1* is directly targeted by individual miRNAs from the miR-379/410 cluster, we cloned a segment of the *Plagl1* 3′ UTR that contained an Ago2 CLIP peak overlapping seed sites for miR-369-3p, miR-376c-3p, and miR-381-3p into a luciferase reporter plasmid. We observed significant repression of luciferase activity upon overexpression of miR-369 ($p = 0.001$) but not upon overexpression of miR-376c or miR-381 (Figures 3E and S3I). This effect was diminished when the 7-mer seed site for miR-369-3p was deleted (Figure 3F), indicating direct regulation of *Plagl1* by this maternally expressed miRNA.

Because imprinted genes are dysregulated in $Mirg^{\Delta/+}$ cells, we asked if imprinting at the *Meg3/Dlk1* locus is altered by maternal miR-379/410 deletion. The *Meg3/Dlk1* intergenic differentially methylated region (IG-DMR) is typically methylated on the paternal allele, and a strong paternal bias in methylation was observed in both $Mirg^{fl/+}$ and $Mirg^{\Delta/+}$ cells (Figure S3J). Accordingly, proper imprinted expression of *Meg3* and *Dlk1* was maintained upon miR-379/410 deletion (Figures S3K and S3L), suggesting these miRNAs do not have a cis-regulatory role in *Meg3/Dlk1* imprinting.

miR-379/410 Regulates Genes Involved in Synaptic Transmission and Neuronal Function

Since miR-379/410 targets are de-repressed in $Mirg^{\Delta/+}$ iNs, including transcriptional regulators like Plagl1 and NeuroD1, we analyzed the global transcriptome upon maternal miR-379/410 deletion by rRNA-depleted RNA-seq. We observed few transcriptional changes in ESCs where miR-379/410 activity is relatively low, but upon differentiation, 332 genes were differentially expressed in $Mirg^{\Delta/+}$ iNs (padj ≤ 0.05, fold change ≥ 2) (Figure 4A; Table S2). We performed gene set enrichment analysis to identify gene ontology terms associated with up- or downregulated genes. Gene sets associated with synaptic transmission, such as action potential and membrane depolarization, were enriched in upregulated genes (Figure 4B). Leading edge analysis highlighted a group of transcripts encoding neurotransmitter receptors and synaptic proteins upregulated upon maternal miR-379/410 deletion (Figure 4C, left). Among these transcripts are components of the glutamatergic signaling pathway, including pre-synaptic vesicular glutamate transporters (*Slc17a6* and *Slc17a7*) and post-synaptic ionotropic glutamate receptors (*Gria4*, *Grid2*, *Grik1*, and *Grin1*) and metabotropic glutamate receptors (*Grm5*, *Grm7*, and *Grm8*). The transcripts encoding *Syn2* and *Syn3*, synaptic vesicular proteins that regulate neurotransmitter release, were also upregulated in $Mirg^{\Delta/+}$ iNs.

Gene set enrichment analysis also highlighted a group of upregulated transcripts implicated in feeding behavior (Figure 4C, right). $Mirg^{\Delta/+}$ iNs expressed higher levels of *Mrap2*, *Mchr1*, *Glp1r*, *Npy2r*, and *Galr2*, neuronal genes that facilitate the effects of nutrient signals on appetite control (Baggio and Drucker, 2014; Georgescu et al., 2005; Naveilhan et al., 1999; Srisai et al., 2017). These data indicate that a nutrient responsive

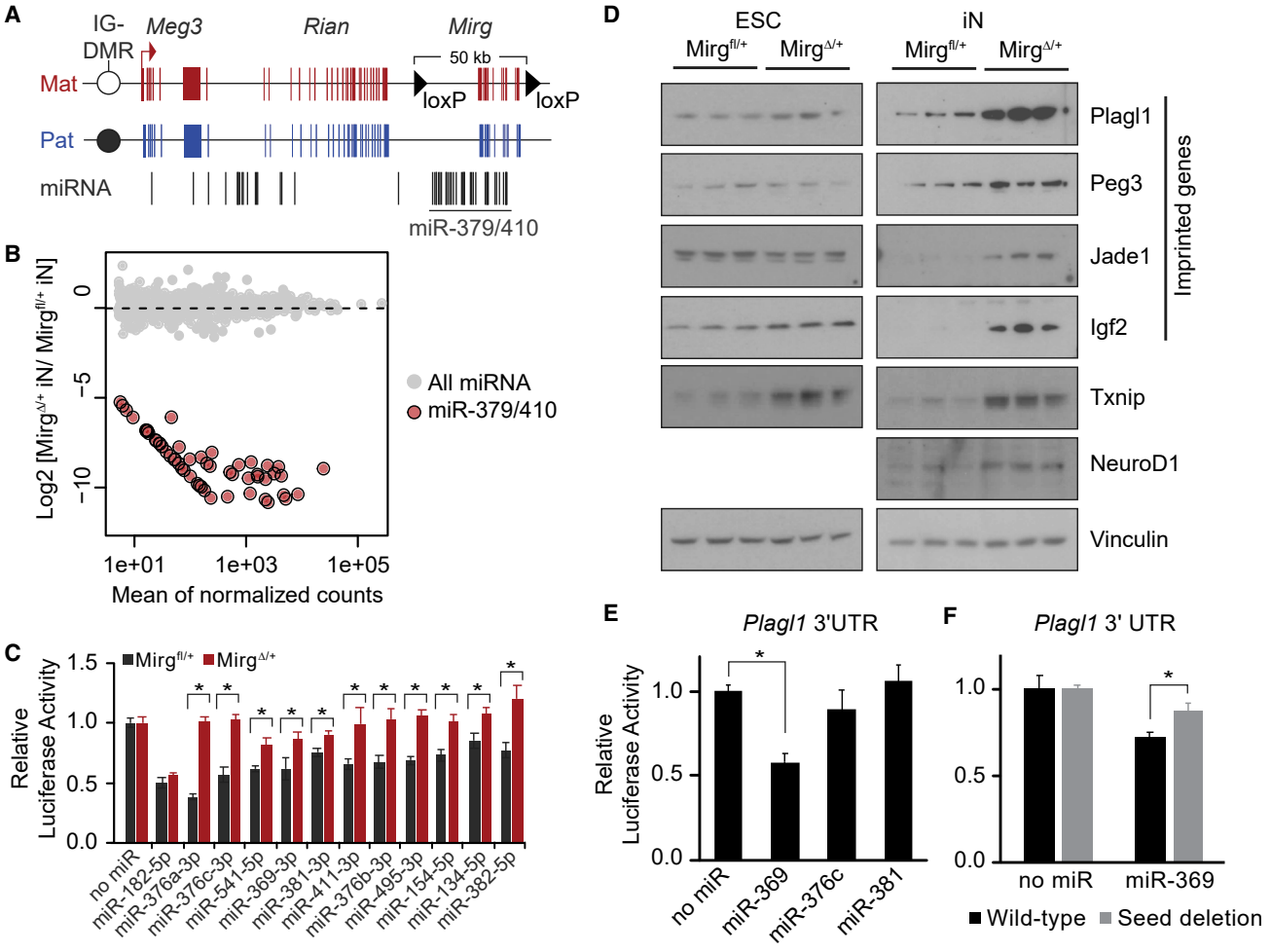

Figure 3. miR-379/410 Targets Are De-repressed upon Maternal miR-379/410 Deletion

(A) Schematic of the *Meg3* genomic locus showing location of maternal loxP insertions flanking the miR-379/410 cluster. IG-DMR, intergenic differentially methylated region.

(B) Expression changes of miRNAs upon maternal deletion of miR-379/410 shown as an MA plot. Gray, all miRNAs; red, miRNA-379/410.

(C) Bar graph of Firefly luciferase activity with or without 3′ UTR miRNA target sites relative to Renilla luciferase internal control. Black, $Mirg^{fl/+}$ iNs; red, $Mirg^{\Delta/+}$ iNs; mean ± SEM (n = 6); *p ≤ 0.05.

(D) western blot of protein lysates from $Mirg^{fl/+}$ and $Mirg^{\Delta/+}$ ESCs and iNs probed with the indicated antibodies. Vinculin was used as a loading control. Biological triplicates are shown for each condition.

(E) Bar graph of relative luciferase activity upon overexpression of the indicated miRNAs in $Mirg^{fl/+}$ iNs from a luciferase reporter containing *Plagl1* 3′ UTR sequence. Mean ± SEM (n = 6); *p ≤ 0.05.

(F) Same as (E) but with a wild-type or deleted miR-369 seed site in the *Plagl1* 3′ UTR luciferase reporter. Mean ± SEM (n = 6); *p ≤ 0.05. p values were calculated using unpaired two-tailed Student's t test. See also Figures S3 and S4.

pathway may be negatively regulated by maternally expressed miRNAs.

No gene sets associated with neurological processes were enriched in downregulated genes. Gene sets enriched for downregulated genes were driven by a large set of ribosomal protein-coding genes that are subtly downregulated (fold change = 1.1–1.4) in $Mirg^{\Delta/+}$ iNs.

We next asked if any transcriptional changes in $Mirg^{\Delta/+}$ iNs can be attributed to the de-repression of the direct miR-379/410 targets Plagl1 and NeuroD1. Transcriptional targets of Plagl1 were previously identified by Plagl1 overexpression in Neuro-2a cells *in vitro* (Varrault et al., 2017) and in mouse cortical neurons *in vivo* (Rraklli et al., 2016; Varrault et al., 2017). We found a significant upregulation of Plagl1-induced transcripts in $Mirg^{\Delta/+}$ iNs ($p < 10^{-8}$) as well as brain tissue from Mirg knockout mice ($p < 10^{-16}$) (Figure 4D), consistent with the increased level of Plagl1 protein in $Mirg^{\Delta/+}$ iNs. Plagl1-induced transcripts that are upregulated upon maternal miR-379/410 deletion include *Synpo*, *Shank1*, and *Sncb*, which function at the synapse. Lastly, the targets of NeuroD1 transcriptional activation (Pataskar et al., 2016) are also significantly upregulated in $Mirg^{\Delta/+}$ iNs ($p < 10^{-16}$) (Figure 4E). Together, these data show that maternally expressed miRNAs have both primary and secondary effects on pathways involved in synaptic activity and neuronal function.

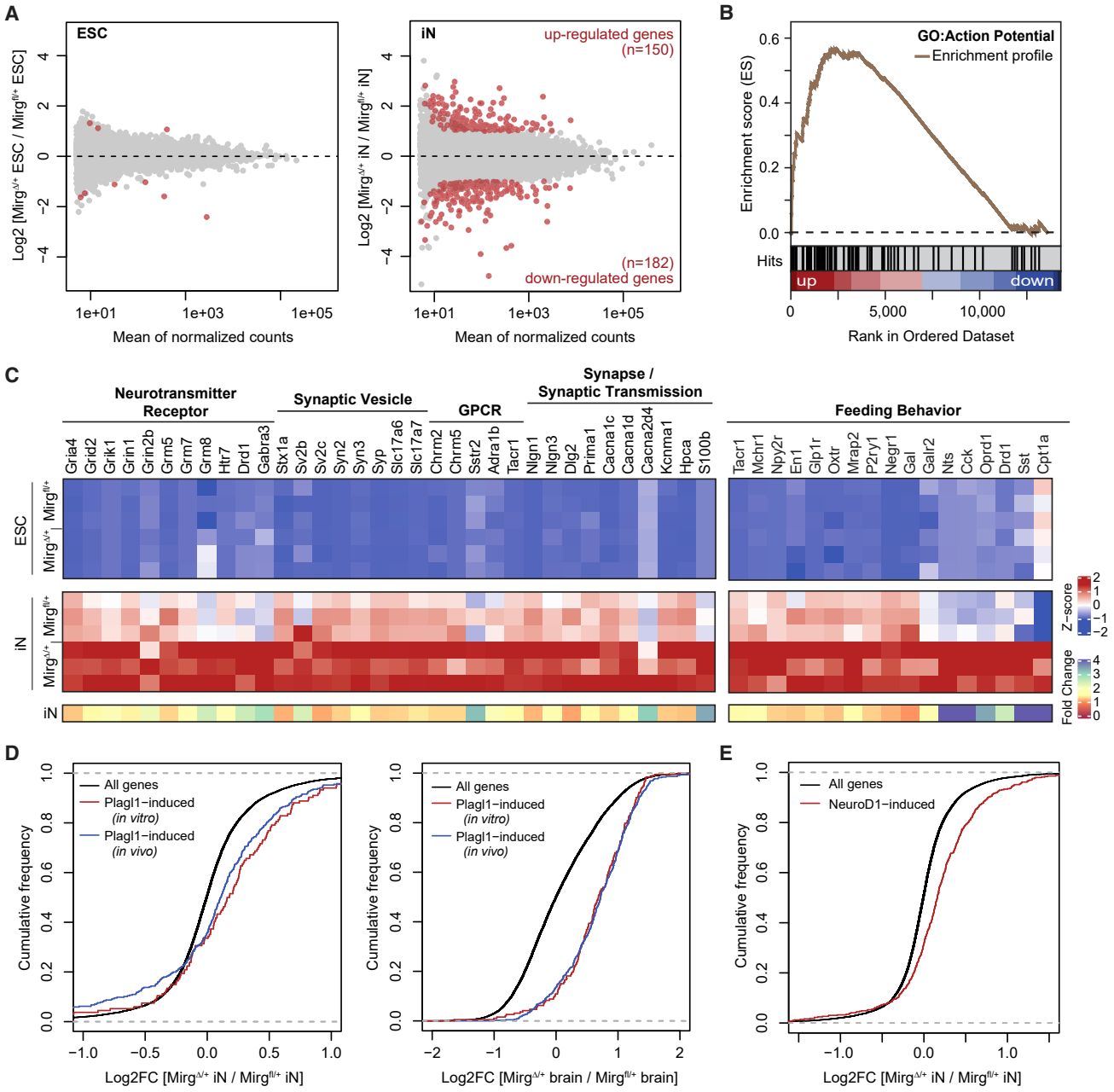

Figure 4. miR-379/410 Regulates Genes Involved in Synaptic Transmission and Neuronal Function

(A) mRNA expression changes in Mirg$^{\Delta/+}$ iNs relative to Mirg$^{fl/+}$ ESCs (left) and iNs (right) shown as MA plots. Gray, all mRNAs; red, differentially expressed mRNAs ($p \leq 0.05$, fold change ≥ 2).

(B) Enrichment profile from gene set enrichment analysis for gene ontology (GO) term "action potential" (normalized enrichment score = 1.88, FDR q-value = 0.11). Genes were ranked from most upregulated to most downregulated in Mirg$^{\Delta/+}$ iNs relative to Mirg$^{fl/+}$ iNs.

(C) Heatmap of core enriched genes associated with synaptic activity and feeding behavior. *Z* scores were calculated based on expression of each gene in Mirg$^{fl/+}$ and Mirg$^{\Delta/+}$ ESCs and iNs (n = 3 for each condition). The fold change in gene expression of Mirg$^{\Delta/+}$ iNs relative to Mirg$^{fl/+}$ iNs is shown in the bottom heatmap.

(D) Left: Cumulative distribution function (CDF) plot of gene expression upon miR-379/410 deletion in iNs for all genes (black, n = 14,325), genes induced by *Plagl1* overexpression in Neuro-2a cells (Varrault et al., 2017) (red, n = 134, $p = 1.8 \times 10^{-8}$), and genes induced by *Plagl1* overexpression in mouse cortical neurons (Rraklli et al., 2016) (blue, n = 356, $p = 8.1 \times 10^{-11}$). Right: CDF plot of gene expression in Mirg knockout mouse brain tissue (see Lackinger et al., 2019) for all genes (black, n = 15,848), genes induced by Plagl1 *in vitro* (red, n = 193, $p < 2.2 \times 10^{-16}$), and genes induced by Plagl1 *in vivo* (blue, n = 446, $p < 2.2 \times 10^{-16}$).

(E) CDF plot of gene expression upon miR-379/410 deletion in iNs for all genes (black, n = 14,325) and genes induced by NeuroD1 (Pataskar et al., 2016) (red, n = 615, $p < 2.2 \times 10^{-16}$). p values in (D) and (E) were calculated using two-sided Kolmogorov-Smirnov test. See also Table S2.

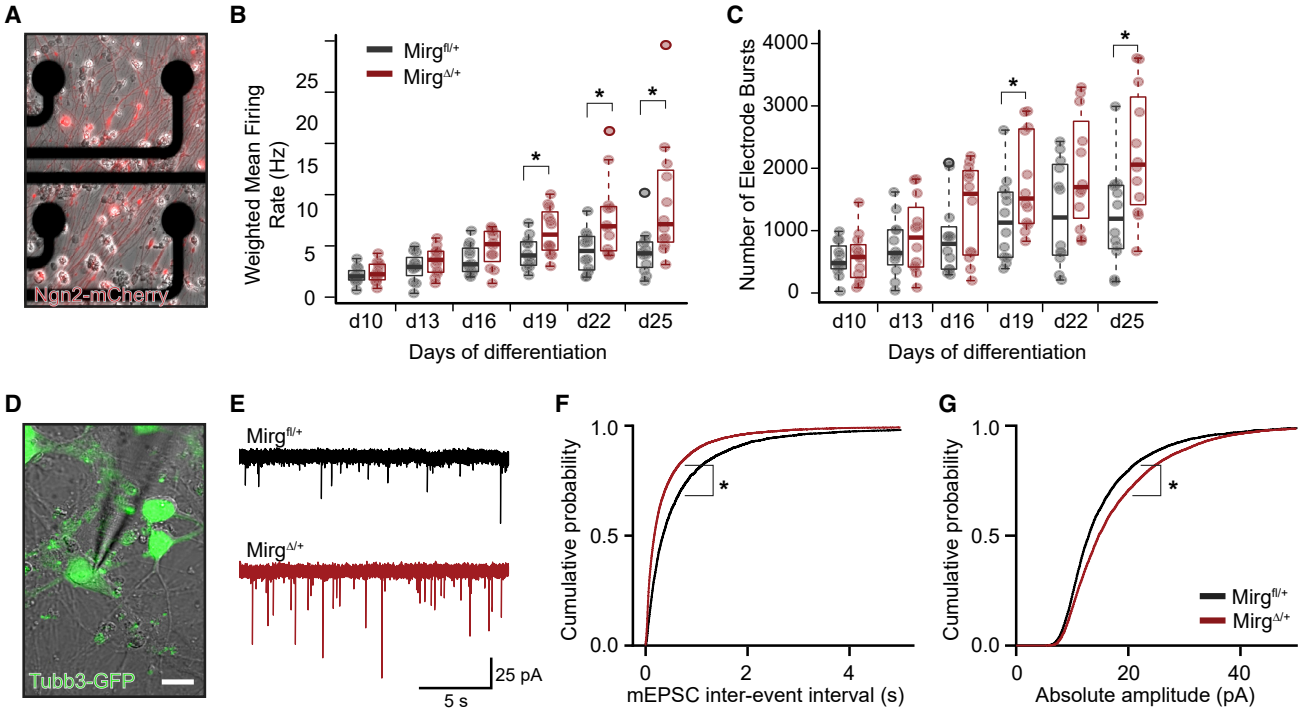

Figure 5. Increased Frequency and Amplitude of Synaptic Events upon Maternal miR-379/410 Deletion

(A) Overlay of brightfield and Ngn2-mCherry fluorescence image of iNs growing on multielectrode array (MEA) plate.

(B) Boxplot of weighted mean firing rate and

(C) electrode bursts from MEA recordings at day 10 to 25 of differentiation. Individual data points are the mean of 16 electrodes in a single well. Black, $Mirg^{fl/+}$ iNs (n = 12 wells); red, $Mirg^{\Delta/+}$ iNs (n = 12 wells); *p $\leq$ 0.05, calculated using unpaired two-tailed Student's t test.

(D) Overlay of differential interference contrast (DIC) image and Tubb3-GFP fluorescence for one example recorded iN. Scale bar, 10 μm.

(E) Example voltage-clamp recordings of miniature excitatory post-synaptic events (mEPSCs) in $Mirg^{fl/+}$ and $Mirg^{\Delta/+}$ iNs.

(F and G) (F) CDF plot of mEPSC inter-event interval ($p = 10^{-98}$) and (G) amplitude ($p = 10^{-37}$) for n = 4,459 and 7,752 events in $Mirg^{fl/+}$ and $Mirg^{\Delta/+}$ iNs, respectively. p values were calculated using two-sided Kolmogorov-Smirnov test. See also Figure S5.

Increased Frequency and Amplitude of Synaptic Events upon Maternal miR-379/410 Deletion

Transcripts involved in synaptic transmission are upregulated in $Mirg^{\Delta/+}$ iNs, so we asked if maternal miR-379/410 deletion affects synaptic activity. $Mirg^{fl/+}$ and $Mirg^{\Delta/+}$ iNs were co-cultured with astrocytes under physiological glucose levels and electrophysiology was assessed using two independent techniques, multielectrode array (MEA) and patch clamp. First, electrical activity was measured in $Mirg^{fl/+}$ and $Mirg^{\Delta/+}$ iNs by changes in the extracellular field potential on MEA plates (Figure S5A). Mature $Mirg^{\Delta/+}$ iNs (day 19 to 25) showed increased electrical activity as indicated by the significant increase in mean firing rate and electrode bursts (Figures 5B and 5C). A similar trend toward increased mean firing rate was observed in a second subclonal cell line (Figure S5A). Second, we performed whole-cell patch clamp recordings on $Mirg^{fl/+}$ and $Mirg^{\Delta/+}$ iNs (day 19 to 22). We recorded miniature excitatory post-synaptic activity (mEPSC) by performing voltage-clamp recordings in the presence of tetrodotoxin and bicuculline to block Na^+ currents and $GABA_A$ transmission, respectively (Figures 5D and 5E). In $Mirg^{\Delta/+}$ iNs, we observed a decrease in the inter-event interval of mEPSCs and, consequently, an increase in mEPSC frequency (Figures 5F and S5B). We also observed increased mEPSC amplitude in $Mirg^{\Delta/+}$ iNs (Figures 5G and S5B). Maternal miR-379/410 deletion does not disturb the membrane properties of iNs, as assessed by unaltered Na^+ and K^+ conductance, spiking activity, and resting membrane potential (Figures S5C–S5F). According to both the MEA and patch clamp recordings, these results collectively demonstrated increased excitatory synaptic transmission upon maternal miR-379/410 deletion.

DISCUSSION

In this study, we generated a robust model system for studying imprinted miRNA activity in neurons by Ngn2-induced differentiation of hybrid ESCs. We performed a comprehensive characterization of maternally expressed miRNAs and discovered that the miR-379/410 cluster directs the RISC complex to transcriptional and developmental regulators, including paternally expressed transcripts. Maternal deletion of miR-379/410 resulted in derepression of these targets, transcriptional upregulation of gene programs associated with synaptic transmission, and increased synaptic activity. We found that a subset of the transcriptional changes observed in $Mirg^{\Delta/+}$ iNs, including several transcripts encoding synaptic proteins, can be attributed to increased levels of the paternally expressed transcriptional

regulator Plagl1. Interestingly, *Plagl1* belongs to a network of co-varying imprinted genes which includes *Meg3*, *Peg3*, and *Igf2* (Varrault et al., 2006, 2017). Our data show that miRNAs co-transcribed from the maternal *Meg3* locus repress *Plagl1*, *Peg3*, and *Igf2*, suggesting miR-379/410 may function as a master coordinator of this imprinted network.

One widely cited evolutionary theory of genomic imprinting, known as the parental conflict or kinship theory, posits that the two parental genomes within offspring have opposing interests in the distribution of maternal resources (Haig and Westoby, 1989; Moore and Haig, 1991). Paternally expressed genes, such as *Igf2*, tend to stimulate nutrient uptake and drive embryonic growth (DeChiara et al., 1991; Ferguson-Smith et al., 1991), whereas maternally expressed genes negatively regulate growth, thereby conserving maternal resources. An example is the maternally expressed *Igf2* receptor, which is a direct functional antagonist of *Igf2* signaling in the placenta (Barlow et al., 1991). The results from our study suggest non-coding RNAs may also actively engage in parental genomic conflict, whereby maternally expressed miRNAs may increase matrilineal inclusive fitness by antagonizing paternally driven gene programs in neurons.

It was previously shown that miR-379/410 knockout mice had an impaired response to changes in nutrient availability during the fetal-neonatal transition and that newborn knockout mice had reduced stomach milk content (Labialle et al., 2014). Defective hepatic gene expression likely accounts, at least in part, for the knockout phenotype, but our data suggest that loss of miRNA activity in the brain could also contribute to the observed impairment in energy homeostasis. Changes in nutrient environment have been shown to increase the frequency of action potentials in hypothalamic neurons through an $AMPA_R$-dependent mechanism (Yang et al., 2011). In our patch clamp studies, we recorded mostly $AMPA_R$-mediated mEPSCs by blocking $NMDA_R$ activity via the addition of 1 mM Mg^{2+} to the bath solution and holding the cells at a negative potential (−70 mV). We observed increased frequency and amplitude of synaptic events in miR-379/410 deletion iNs. While hypothalamic synaptic activity has not been reported in miR-379/410 knockout mice, *in vitro* recordings of hippocampal neurons also showed increased excitatory synaptic transmission (Lackinger et al., 2019). In the future, conditional deletion of maternal miR-379/410 in a stage-specific or neuron subtype-specific manner may help reveal the relative contributions of miRNA dysregulation to metabolic and synaptic phenotypes and may help delineate how potential antagonism between parental genomes shapes organismal development.

There are additional single-copy and clustered miRNAs transcribed from imprinted domains, but further study is needed to determine the selective forces by which they arose. It also remains to be determined what role, if any, maternal-biased Ago2 expression plays in imprinted miRNA activity in the brain. A small group of miRNAs from the upstream region of *Meg3* (miR-127, miR-136, miR-431, miR-433, and miR-434) are transcribed antisense to, and therefore are fully complementary to, the paternally expressed gene *Rtl1*. There is evidence these miRNAs repress *Rtl1* through the RISC pathway (Davis et al., 2005). Our findings demonstrate that a large miRNA cluster from the downstream region of *Meg3* represses paternally expressed transcripts transcribed from distant imprinted loci. The extent to which other imprinted miRNAs regulate imprinted transcripts "in *trans*" will be of great interest.

STAR★METHODS

Detailed methods are provided in the online version of this paper and include the following:

- KEY RESOURCES TABLE
- LEAD CONTACT AND MATERIALS AVAILABILITY
- EXPERIMENTAL MODEL AND SUBJECT DETAILS
  - Cell culture
- METHODS
  - Generation of rtTA;TetO-Ngn2-mCherry;Tubb3-GFP cell line
  - Generation of $Mirg^{fl/+}$ and $Mirg^{\Delta/+}$ cell lines
  - Generation of untagged-Ago2 and HA-Ago2 cell lines
  - Generation of miRNA overexpression cell lines
  - Flow cytometry and fluorescence activated cell sorting (FACS)
  - Fluorescence Imaging
  - Cell confluency measurement
  - Luciferase assay on perfect miRNA targets sites
  - Luciferase assay on wild-type and seed mutant 3′ UTR reporters
  - miRNA qRT-PCR
  - Taqman qRT-PCR
  - Allele-specific qRT-PCR
  - RIP-qRT-PCR
  - Northern blot
  - Western blot
  - Allele-specific DNA methylation
  - Multielectrode array (MEA)
  - Patch clamp electrophysiology
  - Neuron differentiation for sequencing libraries
  - Small RNA-seq, library preparation
  - Small RNA-seq, data analysis pipeline
  - rRNA-depleted RNA-seq, library preparation
  - rRNA-depleted RNA-seq, data analysis pipeline
  - seCLIP-seq, library preparation
  - seCLIP-seq, data analysis pipeline
  - Metagene analysis
  - Biological network of miR-379/410 targets using Cytoscape
  - Analysis of *in vivo* Mirg and miR-379/410 expression
- QUANTIFICATION AND STATISTICAL ANALYSIS
- DATA AND CODE AVAILABILITY

SUPPLEMENTAL INFORMATION

Supplemental Information can be found online at https://doi.org/10.1016/j.molcel.2020.01.020.

ACKNOWLEDGMENTS

We thank R. Jaenisch for sharing the hybrid ESC line used in these studies and access to the multielectrode array and pyrosequencer. We thank the Koch

Institute's Robert A. Swanson Biotechnology Center for technical support, specifically the Flow Cytometry Core, the Genomics Core, and the Barbara K. Ostrom Bioinformatics and Computing Facility. This research was supported by NIH grants P01-CA042063 (P.A.S.), R01-GM034277 (P.A.S.), R01-CA133404 (P.A.S.), R01-EY007023 (M.S.), R01-EY028219 (M.S.), R01-NS090473 (M.S.), and the NCI Koch Institute Cancer Center Support (Core) Grant P30-CA14051. Additional support was provided by postdoctoral fellowships NIH F32HD090833 (A.J.W.), FRQS 31677 (V.B.-P.), and NSERC PDF-48724-2016 (V.B.-P.).

AUTHOR CONTRIBUTIONS

Conceptualization, A.J.W. and P.A.S.; Methodology, A.J.W. and V.B.-P.; Investigation: A.J.W., V.B.-P., H.N.J., and U.K.C.; Writing- Original Draft, A.J.W., and V.B.-P.; Visualization, A.J.W.; Supervision, M.S. and P.A.S.; Funding Acquisition, A.J.W., V.B.-P., M.S., and P.A.S.

DECLARATION OF INTERESTS

The authors declare no competing interests.

Received: August 5, 2019
Revised: December 3, 2019
Accepted: January 15, 2020
Published: February 6, 2020

REFERENCES

Abreu, A.P., Dauber, A., Macedo, D.B., Noel, S.D., Brito, V.N., Gill, J.C., Cukier, P., Thompson, I.R., Navarro, V.M., Gagliardi, P.C., et al. (2013). Central precocious puberty caused by mutations in the imprinted gene MKRN3. N. Engl. J. Med. *368*, 2467–2475.

Agarwal, V., Bell, G.W., Nam, J.-W., and Bartel, D.P. (2015). Predicting effective microRNA target sites in mammalian mRNAs. eLife *4*, e05005.

Al Adhami, H., Evano, B., Le Digarcher, A., Gueydan, C., Dubois, E., Parrinello, H., Dantec, C., Bouschet, T., Varrault, A., and Journot, L. (2015). A systems-level approach to parental genomic imprinting: the imprinted gene network includes extracellular matrix genes and regulates cell cycle exit and differentiation. Genome Res. *25*, 353–367.

Andergassen, D., Dotter, C.P., Wenzel, D., Sigl, V., Bammer, P.C., Muckenhuber, M., Mayer, D., Kulinski, T.M., Theussl, H.-C., Penninger, J.M., et al. (2017). Mapping the mouse Allelome reveals tissue-specific regulation of allelic expression. eLife *6*, e146.

Baggio, L.L., and Drucker, D.J. (2014). Glucagon-like peptide-1 receptors in the brain: controlling food intake and body weight. J. Clin. Invest. *124*, 4223–4226.

Barlow, D.P., Stöger, R., Herrmann, B.G., Saito, K., and Schweifer, N. (1991). The mouse insulin-like growth factor type-2 receptor is imprinted and closely linked to the Tme locus. Nature *349*, 84–87.

Bartel, D.P. (2018). Metazoan MicroRNAs. Cell *173*, 20–51.

Beauparlant, C.J., Lamaze, F.C., Samb, R., Lippens, C., Deschenes, A.L., and Droit, A. (2019). metagene: A package to produce metagene plots. R package, version 2.18.0.

Blouet, C., and Schwartz, G.J. (2011). Nutrient-sensing hypothalamic TXNIP links nutrient excess to energy imbalance in mice. J. Neurosci. *31*, 6019–6027.

Bonthuis, P.J., Huang, W.-C., Stacher Hörndli, C.N., Ferris, E., Cheng, T., and Gregg, C. (2015). Noncanonical genomic imprinting effects in offspring. Cell Rep. *12*, 979–991.

Curley, J.P., Pinnock, S.B., Dickson, S.L., Thresher, R., Miyoshi, N., Surani, M.A., and Keverne, E.B. (2005). Increased body fat in mice with a targeted mutation of the paternally expressed imprinted gene Peg3. FASEB J. *19*, 1302–1304.

Davis, E., Caiment, F., Tordoir, X., Cavaillé, J., Ferguson-Smith, A., Cockett, N., Georges, M., and Charlier, C. (2005). RNAi-mediated allelic trans-interaction at the imprinted Rtl1/Peg11 locus. Curr. Biol. *15*, 743–749.

DeChiara, T.M., Robertson, E.J., and Efstratiadis, A. (1991). Parental imprinting of the mouse insulin-like growth factor II gene. Cell *64*, 849–859.

Dobin, A., Davis, C.A., Schlesinger, F., Drenkow, J., Zaleski, C., Jha, S., Batut, P., Chaisson, M., and Gingeras, T.R. (2013). STAR: ultrafast universal RNA-seq aligner. Bioinformatics *29*, 15–21.

Eggan, K., Akutsu, H., Loring, J., Jackson-Grusby, L., Klemm, M., Rideout, W.M., 3rd, Yanagimachi, R., and Jaenisch, R. (2001). Hybrid vigor, fetal overgrowth, and viability of mice derived by nuclear cloning and tetraploid embryo complementation. Proc. Natl. Acad. Sci. USA *98*, 6209–6214.

Ferguson-Smith, A., Cattanach, B., Barton, S., Beechey, C., and Surani, M. (1991). Embryological and molecular investigations of parental imprinting on mouse chromosome 7. Nature *351*, 351667a0.

Fiore, R., Khudayberdiev, S., Christensen, M., Siegel, G., Flavell, S.W., Kim, T.K., Greenberg, M.E., and Schratt, G. (2009). Mef2-mediated transcription of the miR379-410 cluster regulates activity-dependent dendritogenesis by fine-tuning Pumilio2 protein levels. EMBO J. *28*, 697–710.

Georgescu, D., Sears, R.M., Hommel, J.D., Barrot, M., Bolaños, C.A., Marsh, D.J., Bednarek, M.A., Bibb, J.A., Maratos-Flier, E., Nestler, E.J., and DiLeone, R.J. (2005). The hypothalamic neuropeptide melanin-concentrating hormone acts in the nucleus accumbens to modulate feeding behavior and forced-swim performance. J. Neurosci. *25*, 2933–2940.

Gu, Z., Eils, R., and Schlesner, M. (2016). Complex heatmaps reveal patterns and correlations in multidimensional genomic data. Bioinformatics *32*, 2847–2849.

Haig, D. (2014). Coadaptation and conflict, misconception and muddle, in the evolution of genomic imprinting. Heredity (Edinb) *113*, 96–103.

Haig, D., and Westoby, M. (1989). Parent-specific gene expression and the triploid endosperm. Am. Nat. *134*, 147–155.

Kozomara, A., Birgaoanu, M., and Griffiths-Jones, S. (2019). miRBase: from microRNA sequences to function. Nucleic Acids Res. *47* (D1), D155–D162.

Kuchen, S., Resch, W., Yamane, A., Kuo, N., Li, Z., Chakraborty, T., Wei, L., Laurence, A., Yasuda, T., Peng, S., et al. (2010). Regulation of microRNA expression and abundance during lymphopoiesis. Immunity *32*, 828–839.

Labialle, S., Marty, V., Bortolin-Cavaillé, M.-L., Hoareau-Osman, M., Pradère, J.-P., Valet, P., Martin, P.G., and Cavaillé, J. (2014). The miR-379/miR-410 cluster at the imprinted Dlk1-Dio3 domain controls neonatal metabolic adaptation. EMBO J. *33*, 2216–2230.

Lackinger, M., Sungur, A.Ö., Daswani, R., Soutschek, M., Bicker, S., Stemmler, L., Wüst, T., Fiore, R., Dieterich, C., Schwarting, R.K., et al. (2019). A placental mammal-specific microRNA cluster acts as a natural brake for sociability in mice. EMBO Rep. *20*, e46429.

Li, B., and Dewey, C.N. (2011). RSEM: accurate transcript quantification from RNA-Seq data with or without a reference genome. BMC Bioinformatics *12*, 323.

Li, H., Handsaker, B., Wysoker, A., Fennell, T., Ruan, J., Homer, N., Marth, G., Abecasis, G., and Durbin, R.; 1000 Genome Project Data Processing Subgroup (2009). The Sequence Alignment/Map format and SAMtools. Bioinformatics *25*, 2078–2079.

Lovci, M.T., Ghanem, D., Marr, H., Arnold, J., Gee, S., Parra, M., Liang, T.Y., Stark, T.J., Gehman, L.T., Hoon, S., et al. (2013). Rbfox proteins regulate alternative mRNA splicing through evolutionarily conserved RNA bridges. Nat. Struct. Mol. Biol. *20*, 1434–1442.

Martin, M. (2011). CUTADAPT removes adapter sequences from high-throughput sequencing reads. EMBnet J *17*, 10–12.

Marty, V., Labialle, S., Bortolin-Cavaillé, M.-L., Ferreira De Medeiros, G., Moisan, M.-P., Florian, C., and Cavaillé, J. (2016). Deletion of the miR-379/miR-410 gene cluster at the imprinted Dlk1-Dio3 locus enhances anxiety-related behaviour. Hum. Mol. Genet. *25*, 728–739.

Matsuda, T., and Cepko, C.L. (2007). Controlled expression of transgenes introduced by in vivo electroporation. Proc. Natl. Acad. Sci. USA *104*, 1027–1032.

Moore, T., and Haig, D. (1991). Genomic imprinting in mammalian development: a parental tug-of-war. Trends Genet. *7*, 45–49.

Mootha, V.K., Lindgren, C.M., Eriksson, K.-F., Subramanian, A., Sihag, S., Lehar, J., Puigserver, P., Carlsson, E., Ridderstråle, M., Laurila, E., et al. (2003). PGC-1α-responsive genes involved in oxidative phosphorylation are coordinately downregulated in human diabetes. Nat. Genet. *34*, 267–273.

Naveilhan, P., Hassani, H., Canals, J.M., Ekstrand, A.J., Larefalk, A., Chhajlani, V., Arenas, E., Gedda, K., Svensson, L., Thoren, P., and Ernfors, P. (1999). Normal feeding behavior, body weight and leptin response require the neuropeptide Y Y2 receptor. Nat. Med. *5*, 1188–1193.

Noguer-Dance, M., Abu-Amero, S., Al-Khtib, M., Lefèvre, A., Coullin, P., Moore, G.E., and Cavaillé, J. (2010). The primate-specific microRNA gene cluster (C19MC) is imprinted in the placenta. Hum. Mol. Genet. *19*, 3566–3582.

Pataskar, A., Jung, J., Smialowski, P., Noack, F., Calegari, F., Straub, T., and Tiwari, V.K. (2016). NeuroD1 reprograms chromatin and transcription factor landscapes to induce the neuronal program. EMBO J. *35*, 24–45.

Patten, M.M., Ross, L., Curley, J.P., Queller, D.C., Bonduriansky, R., and Wolf, J.B. (2014). The evolution of genomic imprinting: theories, predictions and empirical tests. Heredity (Edinb) *113*, 119–128.

Patten, M.M., Cowley, M., Oakey, R.J., and Feil, R. (2016). Regulatory links between imprinted genes: evolutionary predictions and consequences. Proc. Biol. Sci. *283*, 1824.

Perez, J.D., Rubinstein, N.D., Fernandez, D.E., Santoro, S.W., Needleman, L.A., Ho-Shing, O., Choi, J.J., Zirlinger, M., Chen, S.-K., Liu, J.S., and Dulac, C. (2015). Quantitative and functional interrogation of parent-of-origin allelic expression biases in the brain. eLife *4*, e07860.

Peters, J. (2014). The role of genomic imprinting in biology and disease: an expanding view. Nat. Rev. Genet. *15*, 517–530.

Quarta, C., Fisette, A., Xu, Y., Colldén, G., Legutko, B., Tseng, Y.-T., Reim, A., Wierer, M., Rosa, M., Klaus, V., et al. (2019). Functional identity of hypothalamic melanocortin neurons depends on Tbx3. Nat. Metabolism *1*, 222–235.

Ran, F.A., Hsu, P.D., Wright, J., Agarwala, V., Scott, D.A., and Zhang, F. (2013). Genome engineering using the CRISPR-Cas9 system. Nat. Protoc. *8*, 2281–2308.

Rraklli, V., Södersten, E., Nyman, U., Hagey, D.W., and Holmberg, J. (2016). Elevated levels of ZAC1 disrupt neurogenesis and promote rapid in vivo reprogramming. Stem Cell Res. (Amst.) *16*, 1–9.

Schratt, G.M., Tuebing, F., Nigh, E.A., Kane, C.G., Sabatini, M.E., Kiebler, M., and Greenberg, M.E. (2006). A brain-specific microRNA regulates dendritic spine development. Nature *439*, 283–289.

Seitz, H., Youngson, N., Lin, S.-P., Dalbert, S., Paulsen, M., Bachellerie, J.-P., Ferguson-Smith, A.C., and Cavaillé, J. (2003). Imprinted microRNA genes transcribed antisense to a reciprocally imprinted retrotransposon-like gene. Nat. Genet. *34*, 261–262.

Shannon, P., Markiel, A., Ozier, O., Baliga, N.S., Wang, J.T., Ramage, D., Amin, N., Schwikowski, B., and Ideker, T. (2003). Cytoscape: a software environment for integrated models of biomolecular interaction networks. Genome Res. *13*, 2498–2504.

Spencer, H.G., and Clark, A.G. (2014). Non-conflict theories for the evolution of genomic imprinting. Heredity (Edinb) *113*, 112–118.

Srisai, D., Yin, T.C., Lee, A.A., Rouault, A.A.J., Pearson, N.A., Grobe, J.L., and Sebag, J.A. (2017). MRAP2 regulates ghrelin receptor signaling and hunger sensing. Nat. Commun. *8*, 713.

Stewart, S.A., Dykxhoorn, D.M., Palliser, D., Mizuno, H., Yu, E.Y., An, D.S., Sabatini, D.M., Chen, I.S., Hahn, W.C., Sharp, P.A., et al. (2003). Lentivirus-delivered stable gene silencing by RNAi in primary cells. RNA *9*, 493–501.

Subramanian, A., Tamayo, P., Mootha, V.K., Mukherjee, S., Ebert, B.L., Gillette, M.A., Paulovich, A., Pomeroy, S.L., Golub, T.R., Lander, E.S., and Mesirov, J.P. (2005). Gene set enrichment analysis: a knowledge-based approach for interpreting genome-wide expression profiles. Proc. Natl. Acad. Sci. USA *102*, 15545–15550.

Tanaka, S., Honda, Y., Takaku, S., Koike, T., Oe, S., Hirahara, Y., Yoshida, T., Takizawa, N., Takamori, Y., Kurokawa, K., et al. (2019). Involvement of PLAGL1/ZAC1 in hypocretin/orexin transcription. Int. J. Mol. Med. *43*, 2164–2176.

Tucci, V., Isles, A.R., Kelsey, G., and Ferguson-Smith, A.C.; Erice Imprinting Group (2019). Genomic imprinting and physiological processes in mammals. Cell *176*, 952–965.

Van Nostrand, E.L., Nguyen, T.B., Gelboin-Burkhart, C., Wang, R., Blue, S.M., Pratt, G.A., Louie, A.L., and Yeo, G.W. (2017). Robust, cost-effective profiling of RNA binding protein targets with single-end enhanced crosslinking and immunoprecipitation (seCLIP). Methods Mol. Biol. *1648*, 177–200.

Varrault, A., Gueydan, C., Delalbre, A., Bellmann, A., Houssami, S., Aknin, C., Severac, D., Chotard, L., Kahli, M., Le Digarcher, A., et al. (2006). Zac1 regulates an imprinted gene network critically involved in the control of embryonic growth. Dev. Cell *11*, 711–722.

Varrault, A., Dantec, C., Le Digarcher, A., Chotard, L., Bilanges, B., Parrinello, H., Dubois, E., Rialle, S., Severac, D., Bouschet, T., and Journot, L. (2017). Identification of Plagl1/Zac1 binding sites and target genes establishes its role in the regulation of extracellular matrix genes and the imprinted gene network. Nucleic Acids Res. *45*, 10466–10480.

Wang, Q., Chow, J., Hong, J., Smith, A.F., Moreno, C., Seaby, P., Vrana, P., Miri, K., Tak, J., Chung, E.D., et al. (2011). Recent acquisition of imprinting at the rodent Sfmbt2 locus correlates with insertion of a large block of miRNAs. BMC Genomics *12*, 204.

Yang, Y., Atasoy, D., Su, H.H., and Sternson, S.M. (2011). Hunger states switch a flip-flop memory circuit via a synaptic AMPK-dependent positive feedback loop. Cell *146*, 992–1003.

Zhang, Y., Pak, C., Han, Y., Ahlenius, H., Zhang, Z., Chanda, S., Marro, S., Patzke, C., Acuna, C., Covy, J., et al. (2013). Rapid single-step induction of functional neurons from human pluripotent stem cells. Neuron *78*, 785–798.

Zhang, Y., Chen, K., Sloan, S.A., Bennett, M.L., Scholze, A.R., O'Keeffe, S., Phatnani, H.P., Guarnieri, P., Caneda, C., Ruderisch, N., et al. (2014). An RNA-sequencing transcriptome and splicing database of glia, neurons, and vascular cells of the cerebral cortex. J. Neurosci. *34*, 11929–11947.

STAR★METHODS

KEY RESOURCES TABLE

REAGENT or RESOURCE	SOURCE	IDENTIFIER
Antibodies		
Rabbit monoclonal anti-Ago2	Cell Signaling Technology	Cat#2897; RRID: AB_2096291
Rat monoclonal anti-HA High Affinity	Roche	Cat#11867423001; RRID: AB_390918
Rabbit polyclonal anti-Enolase-I	Cell Signaling Technology	Cat#3810; RRID: AB_2246524
Rabbit polyclonal anti-Plagl1	Abcam	Cat#ab90472; RRID: AB_2050189
Rabbit polyclonal anti-Peg3	Abcam	Cat#ab99252; RRID: AB_10864541
Rabbit polyclonal anti-Jade-1	Novus	Cat#NBP1-83085; RRID: AB_11024938
Rabbit polyclonal anti-Igf2	Thermo	Cat#PA5-71494; RRID: AB_2717348
Rabbit monoclonal anti-Txnip	Cell Signaling Technology	Cat#14715; RRID: AB_2714178
Rabbit monoclonal anti-NeuroD1	Cell Signaling Technology	Cat#4373; RRID:AB_10549071
Mouse monoclonal anti-Vinculin	Sigma	Cat#V9131; RRID: AB_477629
Sheep anti-mouse IgG-HRP	GE Healthcare	Cat#NA931; RRID: AB_772210
Donkey anti-rabbit IgG-HRP	GE Healthcare	Cat#NA934; RRID: AB_772206
Chemicals, Peptides, and Recombinant Proteins		
Doxycycline hyclate	Sigma	Cat#D9891
Critical Commercial Assays		
Dual-Glo Luciferase Assay System	Promega	Cat#E2920
Q5 Site-Directed Mutagenesis Kit	NEB	Cat#E0554S
GenElute Mammalian Genomic DNA Miniprep Kit	Sigma	Cat#G1N10
miScript RT Kit	QIAGEN	Cat#218160
miScript SYBR Green PCR Kit	QIAGEN	Cat#218073
EXPRESS One-Step SuperScript qRT-PCR Kit	Thermo	Cat#11781200
EpiTect Bisulfit Kit	QIAGEN	Cat#59104
PyroMark PCR Kit	QIAGEN	Cat#978703
QIAseq miRNA Library Kit	QIAGEN	Cat#331502
KAPA RNA HyperPrep Kit with RiboErase (HMR)	Kapa Biosystems	Cat#KK8560
Deposited Data		
Raw and processed data	This paper	GEO: GSE140838
Unprocessed gel images and additional raw files	This paper	https://doi.org/10.17632/hf4xvtz8t4.1
Mouse reference genome GENCODE release M15 (GRCm38.p5)	The GENCODE Project	https://www.gencodegenes.org/mouse/release_M15.html
miRbase (v21)	Kozomara et al., 2019	ftp://mirbase.org/pub/mirbase/21/; RRID:SCR_003152
TargetScanMouse (v7.2)	Agarwal et al., 2015	http://www.targetscan.org/cgi-bin/targetscan/data_download.cgi?db=mmu_72; RRID:SCR_010845
ENCODE microRNA-seq, mouse tissue (E14.5, P0)	ENCODE Project Consortium	GEO: GSE82739, GSE82730, GSE82822, GSE82532, GSE82490, GSE82478, GSE82749, GSE82708, GSE82864, GSE82558, GSE82982, GSE82633, GSE82873, GSE82585
ENCODE polyA+ RNA-seq, mouse tissue (P0)	ENCODE Project Consortium	GEO: GSE78316, GSE78437, GSE78374, GSE78495, GSE78325, GSE78399, GSE78337
Small RNA-seq, mouse tissue (adult)	Kuchen et al., 2010	GSE21630
RNA-seq, mouse brain cell types	Zhang et al., 2014	GSE52564
Digital gene expression profiling, Neuro-2a cells transfected with Plagl1	Varrault et al., 2017	N/A

(*Continued on next page*)

Continued

REAGENT or RESOURCE	SOURCE	IDENTIFIER
RNA-seq, mouse *in utero* electroporation of Plagl1	Rraklli et al., 2016	N/A
RNA-seq, ectopic NeuroD1 induction for 48 hours in ESCs	Pataskar et al., 2016	GSE65072
Experimental Models: Cell Lines		
Mouse: $F_{1.2\text{-}3}$ ESC: 129/Sv x *M. cast*	Eggan et al., 2001	N/A
Mouse: ESC: $F_{1.2\text{-}3}$;M2rtTA;TetO-Ngn2-mCherry; Tubb3-GFP	This paper	N/A
Mouse: $Mirg^{fl/+}$: $F_{1.2\text{-}3}$;M2rtTA;TetO-Ngn2-mCherry; Tubb3-GFP;$Mirg^{fl/+}$	This paper	N/A
Mouse: $Mirg^{\Delta/+}$: $F_{1.2\text{-}3}$;M2rtTA;TetO-Ngn2-mCherry; Tubb3-GFP;$Mirg^{\Delta/+}$	This paper	N/A
Mouse: $Mirg^{fl/+}$;untag-Ago2: $F_{1.2\text{-}3}$;M2rtTA;TetO-Ngn2-mCherry;Tubb3-GFP;$Mirg^{fl/+}$;untag-Ago2	This paper	N/A
Mouse: $Mirg^{fl/+}$;HA-Ago2: $F_{1.2\text{-}3}$;M2rtTA;TetO-Ngn2-mCherry;Tubb3-GFP;$Mirg^{fl/+}$;HA-Ago2	This paper	N/A
Mouse: $Mirg^{\Delta/+}$;miR-369: $F_{1.2\text{-}3}$;M2rtTA;TetO-Ngn2-mCherry;Tubb3-GFP;$Mirg^{\Delta/+}$;miR-369	This paper	N/A
Mouse: primary astrocytes	ScienCell	Cat#M1800
Oligonucleotides		
See Table S3	This paper	N/A
Recombinant DNA		
Plasmid: pSpCas9(BB)-2A-GFP (pX458)	Ran et al., 2013	Cat#48138 Addgene
Plasmid: PB-EF1α-M2rtTA (pAC4)	A.W. Cheng	N/A
Plasmid: PB transposase (mPBase)	A.W. Cheng	N/A
Plasmid: pcDNA3.1 FH-NLS-hAgo2	T. Kelly	N/A
Plasmid: pTetO-Ngn2-Puro	Zhang et al., 2013	Cat#52047 Addgene
Plasmid: pTetO-Ngn2-mCherry	This paper	N/A
Plasmid: pCMV-dR8.2	Stewart et al., 2003	Cat#8455 Addgene
Plasmid: pCMV-VSV-G	Stewart et al., 2003	Cat#8454 Addgene
Plasmid: pCAG-Cre:GFP	Matsuda and Cepko, 2007	Cat#13776 Addgene
Plasmid: PB-EF1α-MCS-IRES-Neo	System Biosciences	Cat#PB533A-2
Plasmid: pmirGLO	Promega	Cat#E1330
Plasmid: pmirGLO-miR.target.site	This paper	N/A
Plasmid: pmirGLO-Plagl1.3′UTR	This paper	N/A
Plasmid: pmirGLO-Plagl1.3′UTR.Del	This paper	N/A
Plasmid: pmirGLO-Neurod1.3′UTR	This paper	N/A
Plasmid: pmirGLO-Neurod1.3′UTR.Del	This paper	N/A
Software and Algorithms		
BD FACSDiva Software (v8.0)	BD Biosciences	RRID:SCR_001456
FlowJo (v9)	FlowJo	RRID:SCR_008520
NEBaseChanger (v1.2.9)	NEB	https://nebasechanger.neb.com/
pCLAMP10 with Clampfit (v10.7) Software	Molecular Devices	RRID:SCR_011323
MATLAB (vR2018b)	MathWorks	RRID:SCR_001622
R (v3.5.1)	R Project	https://www.r-project.org/; RRID:SCR_001905
ComplexHeatmap (v1.20.0) R package	Gu et al., 2016	https://bioconductor.org/packages/release/bioc/html/ComplexHeatmap.html; RRID:SCR_017270
Metagene (v2.14.0) R package	Beauparlant et al., 2019	https://bioconductor.org/packages/release/bioc/html/metagene.html
STAR (v2.4.1)	Dobin et al., 2013	https://github.com/alexdobin/STAR; RRID:SCR_015899

(*Continued on next page*)

Continued

REAGENT or RESOURCE	SOURCE	IDENTIFIER
RSEM (v1.2.30)	Li and Dewey, 2011	https://github.com/deweylab/RSEM; RRID:SCR_013027
DESeq2	https://www.bioconductor.org	RRID:SCR_015687
Samtools	Li et al., 2009	http://samtools.sourceforge.net/; RRID:SCR_002105
Cutadapt (v1.4.2)	Martin, 2011	https://cutadapt.readthedocs.io/en/stable/; RRID:SCR_011841
Fastxtoolkit (v0.0.13)	N/A	http://hannonlab.cshl.edu/fastx_toolkit/
CLIPper	Lovci et al., 2013	https://github.com/YeoLab/clipper
GSEA	Subramanian et al., 2005; Mootha et al., 2003	RRID:SCR_003199
Cytoscape (v3.7.1)	Shannon et al., 2003	RRID:SCR_003032

LEAD CONTACT AND MATERIALS AVAILABILITY

Further information and requests for resources and reagents should be directed to and will be fulfilled by the Lead Contact, Amanda J. Whipple (amanda_whipple@fas.harvard.edu).

EXPERIMENTAL MODEL AND SUBJECT DETAILS

Cell culture

Cell line maintenance

The ESC line used in this study was derived from an F1 *Mus. musculus* x *Mus. castaneous* cross ($F_{1.2\text{-}3}$, (Eggan et al., 2001)). ESCs were adapted to feeder-free conditions by 10 passages on tissue culture plates pre-coated with 0.2% gelatin in phosphate-buffered saline (PBS). For routine passaging, cells were washed in HEPES buffered saline (HBS), dissociated using 0.25% trypsin-EDTA, and then plated on gelatin-coated plates in ESC medium [Dulbecco's Modified Essential Media (Thermo) containing 10 mM HEPES (Thermo), 15% HyClone fetal bovine serum (Thermo), 1000 U/mL leukemia inhibitory factor (Millipore Sigma), 0.11 mM β-mercaptoethanol (Sigma), 1X non-essential amino acids (Thermo), 2 mM L-glutamine (Thermo), 1X penicillin streptomycin solution (Corning)]. Cells were maintained in a humidified 5% CO_2 incubator at 37°C.

Neuron differentiation

ESC lines stably expressing rtTA and TetO-Ngn2 (see below) were cultured for 24 hours on gelatin-coated tissue culture plates in N2B27 medium [1:1 ratio of DMEM/F12 + Glutamax (Thermo) and Neurobasal Medium (Thermo), supplemented with 1X N2 supplement (Thermo), 1X B27 supplement minus Vitamin A (Thermo), 0.5X non-essential amino acids (Thermo), 1 mM L-glutamine (Thermo), 1X penicillin streptomycin solution (Corning), 0.05 mM β-mercaptoethanol (Sigma), 0.5 mM sodium pyruvate (Thermo), 0.02% BSA Fraction V (Thermo), 0.25 ug/mL laminin (Thermo), 10 ng/mL BDNF (Sigma), 10 ng/mL NT3 (R&D Systems), 1 ug/mL doxycycline (Sigma)]. Then, cells were dissociated using accutase (STEMCELL Technologies) and 6×10^5 cells were plated on PEI-coated six-well plates (0.1% PEI in borate buffer). Borate buffer contains 50 mM boric acid (Sigma) and 24 mM sodium tetraborate (Sigma) at pH 8.4. One half of the medium was replaced every two days. iNs were harvested at day 10 unless otherwise noted.

METHODS

Generation of rtTA;TetO-Ngn2-mCherry;Tubb3-GFP cell line

First, GFP was knocked in to the endogenous Tubb3 locus to serve as a marker of differentiation. A single guide RNA (sgRNA) targeted to the Tubb3 3′ UTR (Tubb3sg Fwd/Rev, Table S3) was cloned into pX458 (Addgene), then co-transfected with a homology-directed repair (HDR) template, P2A-eGFP-T2A-Puro flanked by 450 bp homology arms, into $F_{1.2\text{-}3}$ ESCs using Lipofectamine 2000 (Thermo). Transfected cells were re-plated at a low density and single cell clones were manually isolated. Genomic DNA was prepared using Quick Extract (Epicenter) and a single cell clone with successful insertion of Tubb3-P2A-GFP-T2A-Puro was confirmed by PCR. Second, the PiggyBac pAC4 vector (co-expressing EF1α-M2rtTA and CMV-Hygro, gifted from A.W. Cheng) was co-transfected with mPBase plasmid (expressing the PiggyBac transposase, A.W. Cheng) into Tubb3-GFP ESCs. Cells with stable integration of rtTA were selected in the presence of 150 ug/mL Hygromycin B for 10 days. Third, the lentiviral pTetO-Ngn2-Puro plasmid (Addgene) was modified to pTetO-Ngn2-mCherry using Gibson Assembly (NEB). Lentivirus was produced in HEK293 cells by co-transfection of pTetO-Ngn2-mCherry, pCMV-dR8.2 (Addgene), and pCMV-VSV-G (Addgene) using TransIT-LT1 Transfection Reagent (Mirus). Viral-containing supernatant was applied to rtTA;Tubb3-GFP ESCs in the presence of 5 ug/mL polybrene (Sigma).

An infected single cell clone (rtTA;TetO-Ngn2-mCherry;Tubb3-GFP) was identified and confirmed by mCherry/GFP fluorescence following doxycycline treatment.

Generation of $Mirg^{fl/+}$ and $Mirg^{\Delta/+}$ cell lines

sgRNAs (Mirg.up sgFwd/Rev and Mirg.dn sgFwd/Rev, Table S3) were designed to sites flanking the miR-379/410 cluster and were cloned into the pX458 plasmid (Addgene). HDR templates containing a loxP site flanked by 60 bp homology arms were designed to each sgRNA site and were synthesized as single-stranded oligonucleotides (IDT) (Mirg.up HDR template and Mirg.dn HDR template, Table S3). sgRNAs and HDR templates were co-transfected into rtTA;TetO-Ngn2-mCherry;Tubb3-GFP ESCs using Lipofectamine2000 (Thermo). Single cells were isolated by FACS into individual wells of a 96-well plate and screened for loxP insertion by PCR at the upstream and downstream insertion sites. A single cell clone with dual loxP insertion was confirmed to be maternal-specific by Sanger sequencing of allelic SNPs within loxP-containing PCR products. Next, the miR-379/410 cluster was deleted by transient transfection of pCAG-Cre:GFP (Addgene). Since cell clones were isolated by FACS for GFP-negative ($Mirg^{fl/+}$) and GFP-positive ($Mirg^{\Delta/+}$) cells, and Cre-mediated deletion of miR-379/410 was confirmed by PCR.

Generation of untagged-Ago2 and HA-Ago2 cell lines

Untagged-Ago2 and HA-Ago2 was amplified by PCR from pcDNA3.1 FH-NLS-hAgo2 plasmid (gifted from T. Kelly) with primers Ago2 Fwd/Rev and HA-Ago2 Fwd/Rev (Table S3), respectively. The PCR products were cloned into the multiple cloning site of the PiggyBac expression vector PB-EF1α-MCS-IRES-Neo (System Biosciences, PB533A-2) by restriction enzyme ligation. Sequence-verified plasmids were co-transfected with mPBase plasmid (expressing the PiggyBac transposase) into $Mirg^{fl/+}$ ESCs using Lipofectamine2000 (Thermo). Cells with stable Ago2 integration were selected in ESC medium containing 300 ug/mL G418 (Sigma) for 10 days.

Generation of miRNA overexpression cell lines

The pri-miRNA sequence for miR-369 was amplified from genomic DNA using the miR369 Fwd/Rev primers (Table S3). It was then cloned into the multiple cloning site of the PiggyBac expression vector PB-EF1α-MCS-IRES-Neo (System Biosciences, PB533A-2) using Gibson Assembly (NEB). Sequence-verified plasmids were co-transfected with mPBase plasmid (expressing the PiggyBac transposase) into $Mirg^{fl/+}$ ESCs using Lipofectamine2000 (Thermo). Cells with stable integration of EF1α-MCS-IRES-Neo (''no miR'' control) or EF1α-miRNA-IRES-Neo were selected in ESC medium containing 300 ug/mL G418 (Sigma) for 10 days.

Flow cytometry and fluorescence activated cell sorting (FACS)

Single cells were sorted using the FACSAria cell sorter (Becton Dickinson) into individual wells of a gelatin-coated 96-well plate containing ESC medium. To analyze the efficiency of neuron differentiation, cells were analyzed on the FACSCelesta (Becton Dickinson) flow cytometry instrument with FACSDiva v8.0 software. FCS files were exported and analyzed with FlowJo v9.

Fluorescence Imaging

Cells were imaged on the Incucyte (Sartorius) live cell imager or ApoTome.2 (Zeiss) fluorescence microscope using the brightfield and mCherry channels.

Cell confluency measurement

$Mirg^{fl/+}$ and $Mirg^{\Delta/+}$ ESCs were plated on a gelatin-coated 12-well plate (40,000 cells/well) in ESC medium (n = 3 wells for each cell line) and maintained inside the Incucyte (Sartorius) live cell imager at 37°C and 5% CO_2. Four brightfield images per well were acquired on the Incucyte every 4 hours for a total of 40 hours. Confluency measurements were automatically calculated by the Incucyte software.

Luciferase assay on perfect miRNA targets sites

Single strand oligonucleotides containing perfect target sites fully complementary to mature miRNAs (GLO.miR Fwd/Rev, Table S3) were annealed and cloned into the multiple cloning site of the pmirGLO dual luciferase expression vector (Promega) using restriction enzyme ligation. Plasmid insertions were verified by Sanger sequencing. $Mirg^{fl/+}$ and $Mirg^{\Delta/+}$ ESCs were plated on gelatin-coated, white-walled 96-well plates at a density of 8,000 cells per well. After 24 hours, cells were transfected with 200 ng pmirGLO plasmid using Lipofectamine2000. Transfection medium was replaced after six hours with N2B27 medium containing 1 ug/mL doxycycline to induce differentiation. After 48 hours of differentiation, the luciferase assay was performed using the reagents and protocol from the Dual-Glo Luciferase Assay System (Promega) according to the manufacturer's instructions. Luminescence was measured on the Infinite 200 (Tecan Life Sciences). For each sample, Firefly luminescence was normalized to Renilla luminescence as an internal expression control. The Firefly/Renilla ratios for each sample were then normalized to pmirGLO containing no miRNA binding site. Six biological replicates were included for each condition.

Luciferase assay on wild-type and seed mutant 3′ UTR reporters

Primers were used to amplify from genomic DNA the 250 bp region surrounding an Ago2 CLIP peak in the *Plagl1* 3′ UTR that overlapped several miR-379/410 seed sites (Plagl1.3′UTR Fwd/Rev, Table S3). These 3′ UTR sequences were then inserted into

the multiple cloning site of the pmirGLO dual luciferase expression vector (Promega) using restriction enzyme ligation. To generate the seed deleted 3′ UTR reporter, the Q5 site directed mutagenesis assay (NEB) was used to delete the miR-369 seed site. Primers for site directed mutagenesis were designed flanking the miR-369 seed site using NEBaseChanger (v1.2.9, NEB) (Plagl1.3′UTRDel Fwd/Rev, Table S3). Sequence-verified luciferase plasmids containing wild-type or seed mutant 3′ UTR sequence were subsequently transfected into $Mirg^{fl/+}$ or $Mirg^{fl/+}$;miR-369 overexpression ESCs according to the luciferase assay conditions described above.

miRNA qRT-PCR

Total RNA was harvested $Mirg^{fl/+}$ and $Mirg^{\Delta/+}$ cells using TRIzol (Thermo) according to the manufacturer's instructions. Reverse transcription was performed using the miScript II RT Kit (QIAGEN) with 500 ng RNA and the miScript HiSpec Buffer, followed by PCR using the miScript SYBR Green PCR Kit (QIAGEN). miRNA-specific forward primers are listed in Table S3.

miRNAs were normalized to U6 and relative expression was calculated using the delta-delta Ct method. The mean and standard error was calculated from biological triplicates.

Taqman qRT-PCR

One-step qRT-PCR was performed using 25 ng DNase-digested RNA from $Mirg^{fl/+}$ and $Mirg^{\Delta/+}$ cells with EXPRESS One-Step SuperScript qRT-PCR Kit (Thermo) on the StepOne qPCR machine (Applied Biosystems). PrimeTime qPCR Probe Assays (IDT, Table S3) were generated to the target of interest normalized to Gapdh. The relative expression was calculated using the delta-delta Ct method. The mean and standard error was calculated from biological triplicates.

Allele-specific qRT-PCR

Taqman SNP genotyping assays (Thermo) were designed to allele-specific SNPs in *Meg3* and *Dlk1* (Meg3.SNP.qPCR and Dlk1.SNP.qPCR, Table S3). One-step qRT-PCR was performed using 100 ng DNase-digested RNA from $Mirg^{fl/+}$ and $Mirg^{\Delta/+}$ cells with EXPRESS One-Step SuperScript qRT-PCR Kit (Thermo) on the StepOne qPCR machine (Applied Biosystems). The Ct values for maternal and paternal amplification were normalized to a standard curve that was generated using known ratio mixtures of maternal-specific and paternal-specific synthetic amplicons (Table S3).

RIP-qRT-PCR

$Mirg^{fl/+}$;untag-Ago2 and $Mirg^{fl/+}$;HA-Ago2 cells were plated on PEI-coated plates (3×10^5 cells per 10 cm plate) and differentiated for six days (see neuron differentiation protocol). Cells were washed in ice cold 1X PBS and lysed for 10 min in ice cold lysis buffer [50 mM Tris-HCl pH 7.4, 100 mM NaCl, 1% NP-40, 0.1% SDS, 0.5% sodium deoxycholate, 0.4 U/uL murine RNase inhibitor (NEB), 1:200 Protease Inhibitor Cocktail (Millipore)]. Cellular debris was pelleted by centrifugation at 14,000 rpm for 10 min at 4°C. 50 uL of anti-HA magnetic beads (Thermo) were blocked in 3% BSA and then incubated with cell lysate at 4°C overnight. Beads were separated with a magnet, washed three times in 500 uL cold lysis buffer, and then resuspended in TRIzol. Following RNA isolation, miRNA immunoprecipitation was measured by qRT-PCR (see miRNA qRT-PCR protocol). Fold enrichment in HA-Ago2 iNs was calculated relative to untag-Ago2 iNs.

Northern blot

Total RNA was harvested using TRIzol (Thermo) according to the manufacturer's instructions. Four micrograms total RNA was diluted in Gel Loading Buffer II (Thermo), heat denatured at 95°C for 5 min, separated on an 8% urea gel (National Diagnostics), and then transferred by semi-dry transfer (300 mA, 60 min) to Amersham Hybond N+ membrane (GE Healthcare). The Northern probes (Table S3) were 5′ end labeled with ATP Gamma ^{32}P (Perkin Elmer) using T4 polynucleotide kinase (NEB), and then hybridized to the membrane overnight in ULTRAhyb-Oligo buffer (Thermo) in a 42°C rotating hybridization oven. The membrane was washed in 2X SSC containing 0.1% SDS three times and then exposed on a Phosphorimager.

Western blot

Whole cell extract was prepared by washing $Mirg^{fl/+}$ and $Mirg^{\Delta/+}$ cells in ice cold 1X phosphate buffered saline (PBS), then lysing in pre-chilled RIPA buffer containing 10 mM Tris-HCl pH 7.4, 100 mM NaCl, 1% Trixon X-100, 0.1% SDS, 1 mM EDTA, and cOmplete, EDTA-free protease inhibitor cocktail (Roche). Cell lysates were rotated for 30 min at 4°C, then cell debris was pelleted at 4°C for 30 min at 12,000 rpm. Protein concentration was determined using the BCA assay (Pierce). 30 ug protein lysates were diluted in 1X NuPAGE LDS Sample Buffer (Thermo) and 1X NuPAGE Reducing Reagent (Thermo), heat denatured at 70°C for 10 min, and separated on NuPAGE 4%–12% Bis-Tris gels in 1X NuPAGE MOPS SDS Running Buffer (Thermo). Following transfer to PVDF membrane in 1X NuPAGE Transfer Buffer (Thermo), membranes were blocked in 5% milk in PBST, and incubated overnight at 4°C in primary antibody [anti-HA high affinity antibody (Roche, 11867423001), Enolase I (Cell Signaling Technologies, 3810S), Vinculin (Sigma, V9131), anti-Plagl1 (Abcam, ab90472), anti-Peg3 (Abcam, ab99252), anti-Jade1 (Novus, NBP1-83085), anti-Igf2 (Thermo, PA5-71494), anti-Txnip (Cell Signaling Technology, 14715S), anti-Ago2 (Cell Signaling Technology, 2897S), anti-NeuroD1 (Cell Signaling Technologies, 4373)]. Membranes were washed in 1X PBST, then incubated at room temperature for 1 hour in HRP-conjugated

secondary antibody [anti-mouse IgG (GE Healthcare NA931V), anti-rabbit IgG (GE Healthcare NA934V)]. Blots were exposed with Western Lightning Plus-ECL (Perkin Elmer) or SuperSignal West Dura Extended Duration Substrate (Thermo).

Allele-specific DNA methylation

Genomic DNA was isolated from $Mirg^{fl/+}$ and $Mirg^{\Delta/+}$ cells using the GenElute Mammalian Genomic DNA Miniprep Kit (Sigma) according to the manufacturer's instructions. Bisulfite conversion was performed on 500 ng genomic DNA using the EpiTect Bisulfite Kit (QIAGEN). M.SssI-treated DNA was used as a positive control for complete bisulfite conversion. PCR was performed on 20 ng bisulfite converted DNA with primers in the IG-DMR that amplify seven bi-allelic CpG sites and one paternal-specific CpG site (CpG Fwd/Bio-Rev, Table S3) using the PyroMark PCR Kit (QIAGEN). Sequencing assays were run on the PyroMark Q48 pyrosequencer (QIAGEN) using the CpG sequencing primer (Table S3). The percent methylation at the paternal-specific CpG site was subtracted from the average percent methylation at non-allelic CpG sites to yield the percent methylation on the maternal allele.

Multielectrode array (MEA)

Primary mouse astrocytes (ScienCell) were expanded on tissue culture flasks pre-coated with 50 ug/mL poly-L-lysine for 3-4 passages in Astrocyte Medium-animal (ScienCell). Classic MEA 48 plates (Axion Biosystems) were pre-coated with 0.1% PEI, then 7×10^5 astrocytes and 7×10^5 $Mirg^{fl/+}$ or $Mirg^{\Delta/+}$ day 1 iNs were mixed and plated in each well by drop placement. For electrophysiology experiments, iNs were cultured in BrainPhys Neuronal medium (StemCell Technologies) containing 10 ng/mL BDNF (Sigma), 1X N2 supplement (Thermo), SM1 Neuronal Supplement (StemCell Technologies), and 1 ug/mL doxycycline (Sigma). Twelve wells were plated per condition. Recordings of spontaneous activity were performed for 10 min at 37°C every 3 days from day 10 to 25 on the MEA Maestro system (Axion Biosystems). Electrode bursts were calculated using the ISI threshold algorithm with minimum number of spikes = 5 and maximum ISI = 100 ms.

Patch clamp electrophysiology

1×10^5 primary mouse astrocytes and 2×10^5 $Mirg^{fl/+}$ or $Mirg^{\Delta/+}$ day 1 iNs were mixed and plated on PEI-coated 15 mm circular coverslips in a 12-well plate. For electrophysiology experiments, iNs were cultured in BrainPhys Neuronal medium (StemCell Technologies) containing 10 ng/mL BDNF (Sigma), 1X N2 supplement (Thermo), SM1 Neuronal Supplement (StemCell Technologies), and 1 ug/mL doxycycline (Sigma). At day 19 to 22, coverslips were placed in a recording chamber (Series 20, Warner Instruments) and perfused at a rate of 1-2 mL/min with room-temperature ACSF containing the following: 140 mM NaCl, 5 mM KCl, 10 mM HEPES, 1 mM $MgSO_4$, 2 mM $CaCl_2$ and 10 mM D-Glucose; pH 7.3-7.4 and osmolarity 300. We used 3-6 MΩ glass pipettes filled with K-Glu-based intracellular solution containing 140 mM K-gluconate, 10 mM KCl, 10 mM HEPES, 1 mM EGTA, 0.1 mM $CaCl_2$, 1 mM Mg-ATP, 1 mM Na_2-GTP, and 4 mM D-Glucose; pH 7.4 and osmolarity 290. iNs were visualized with differential interference contrast (DIC) or fluorescence using a charge-coupled device (CCD) camera (ORCA-R2 C10600, Hamamatsu). Recordings were performed with a Multiclamp 700b (Molecular Devices) amplifier, digitized at 10 kHz, and low-pass filtered at 1 kHz with a Digidata 1440 and pCLAMP10 software (Molecular Devices). To isolate mEPSCs, we added 1 μM TTX (Abcam, ab120055) and 20 μM bicuculline (Tocris, 0131) to the bath solution to block Na^+ and $GABA_A$ currents respectively and cells were voltage-clamped at a membrane potential of −70 mV. Access resistance was 17.6 ± 0.7 and 17.4 ± 0.9 MΩ in $Mirg^{fl/+}$ and $Mirg^{\Delta/+}$ iNs, respectively. mEPSCs, membrane properties, and spiking properties were analyzed using Clampfit software (v10.7, Molecular Devices) and custom MATLAB scripts (vR2018b, MathWorks). mEPSCs properties were calculated over 3-min-long recordings. Spontaneous spiking rate and resting membrane potential were calculated over 1-min-long current-clamp recordings. Evoked spike rate activity was calculated by counting the number of spikes elicited by injecting +50 pA currents during 1 s. Sodium and potassium currents were measured as the peak negative current and the average positive current following the injection of voltage steps (ranging from −90 to 50 mV; 10 mV increments).

Neuron differentiation for sequencing libraries

$Mirg^{fl/+}$ or $Mirg^{\Delta/+}$ ESCs were differentiated according to the neuron differentiation protocol above and total RNA was prepared from three biological replicates of day 10 iNs from each cell line using TRIzol. RNA was treated with DNase I (Thermo) under standard reaction conditions. DNase-treated RNA was used for preparation of small RNA-seq and rRNA-depleted RNA-sequencing libraries.

Small RNA-seq, library preparation

Small RNA-seq libraries were prepared from 100 ng DNase-treated RNA using QIAseq miRNA library kit (QIAGEN) with 16 cycles of PCR amplification. Quality control of final libraries was assessed with a fragment analyzer and qPCR for colony forming units prior to pooling and loading on an Illumina FlowCell (HiSeq2000, 40 bp SE reads). Each sample library was sequenced to a depth of 9-12 M reads.

Small RNA-seq, data analysis pipeline

Adaptor sequences were first trimmed from small RNA-sequencing reads using cutadapt (v1.4.2) with the following command:

```
cutadapt -a AACTGTAGGCACCATCAAT–minimum length 14 $input/ID_sequence.fastq > $input/ID_sequence_trim.fastq 2 > $input/TrimReport-ID.txt
```

Before mapping small RNA-seq reads to the transcriptome, we added all mature miRNA annotations from miRBase (v21) into the mm10 Gencode M15 gtf file. Mature miRNAs were inserted as distinct transcripts of the appropriate parent pri-miRNA gene annotation, allowing STAR alignment and RSEM counting of gene-level and mature miRNA-level counts. STAR (v2.4.1d) was used to map small RNA-sequencing reads to mm10 genome and transcriptome (Gencode M15 assembly containing miRBase annotations) with the following command:

STAR–runThreadN 8–runMode alignReads–genomeDir $genome/–readFilesIn $input/ID_sequence_trim.fastq–outFileNamePrefix $input/ID–outReadsUnmapped Fastx–outSAMtype BAM SortedByCoordinate–outFilterMismatchNoverLmax 0.05–outFilterMatchNmin 16–outFilterScoreMinOverLread 0–outFilterMatchNminOverLread 0–alignIntronMax 1–sjdbGTFfile $gtf/gencode.vM15.miRBase.gtf–sjdbOverhang 74–quantMode TranscriptomeSAM

RSEM (v1.2.30) was used to count transcriptome mapped reads with the following command:

rsem-calculate-expression–bam–forward-prob 0.5 -p 8–no-bam-output–calc-pme–seed-length 16 $input/IDAligned.toTranscriptome.out.bam $genome/GRCm38_GencodeM15_miRBase $input/ID

Quantification of RSEM counts was performed on ID.isoforms.results files using DESeq2. Only mature miRNAs with mean normalized counts $\geq$ 5 were included in the analysis. Differentially expressed miRNAs between $Mirg^{fl/+}$ and $Mirg^{\Delta/+}$ iNs were determined as padj $\leq$ 0.05 and fold change $\geq$ 2. Heatmap of Log2[Normalized counts] were generated using ComplexHeatmap (v1.20.0) package in R. The proportion of total miRNA reads mapping to miR-379/410 miRNAs was calculated in R using the posterior mean counts from RSEM for all mature miRNAs.

rRNA-depleted RNA-seq, library preparation

rRNA-depleted RNA-sequencing libraries were prepared from 400 ng DNase-treated RNA using KAPA RNA HyperPrep Kit with RiboErase (HMR) (Kapa Biosystems) using 9 cycles of PCR amplification. Quality control on final libraries was assessed with a fragment analyzer and qPCR for colony forming units prior to pooling and loading on an Illumina FlowCell (NextSeq 500, 75 bp PE reads). Each sample library was sequenced to a depth of 38-50 M reads.

rRNA-depleted RNA-seq, data analysis pipeline

STAR (v2.4.1d) was used to map RNA-sequencing reads to mm10 genome and transcriptome (Gencode M15 assembly) with the following command:

STAR–runThreadN 8–runMode alignReads–genomeDir $genome/–readFilesIn $input/ID_1.fastq $input/ID_2.fastq–outFileNamePrefix $input/ID–outFilterType BySJout–outReadsUnmapped Fastx–outSAMtype BAM SortedByCoordinate–outFilterMultimapNMax 20–outFilterMismatchNmax 999–outFilterMismatchNoverLmax 0.04–alignIntronMin 70–alignIntronMax 1000000–alignMatesGapMax 1000000–alignSJoverhangMin 8–alignSJBoverhangMin 1–sjdbGTFfile $genome/gencode.vM15.primary_assembly.annotation.gtf–sjdbOverhang 74–twopassMode Basic–quantMode TranscriptomeSAM

RSEM (v1.2.30) was used to count transcriptome mapped reads with the following command:

rsem-calculate-expression–bam–paired-end–forward-prob 0 -p 8–no-bam-output–calc-pme $input/IDAligned.toTranscriptome.out.bam $genome/ $input/rsem/ID

Gene level quantification was performed on RSEM ID.genes.results files using DESeq2. Only genes with mean normalized counts $\geq$ 5 were included in the analysis. Differentially expressed genes between $Mirg^{fl/+}$ and $Mirg^{\Delta/+}$ iNs were determined as padj $\leq$ 0.05 and fold change $\geq$ 2. Gene set enrichment analysis (GSEA) was performed by ranking all genes from most upregulated to most downregulated and enrichment was calculated for the Molecular Signatures Database v6.2 C5 GO gene sets. For the heatmap of GSEA core enriched genes, we first calculated the z-score across samples for each gene based on the transcripts per million (TPM) output from RSEM using the scale function in R. Then, the heatmap was generated using ComplexHeatmap (v1.20.0) R package. The cumulative frequency plot (Figures 4D and 4E) was generated in R (v3.5.1) using the plot.ecdf function. Plagl1-regulated genes *in vitro* (Varrault et al., 2017) or *in vivo* (Rraklli et al., 2016) were defined as all induced genes from overexpression of Plagl1 with padj $\leq$ 0.01 and fold change $\geq$ 2. NeuroD1-induced genes from (Pataskar et al., 2016) were defined as all genes upregulated upon induction of NeuroD1 with padj $\leq$ 0.01 and fold change $\geq$ 2.

To quantify allelic expression of *Meg3* and *Dlk1* from RNA-sequencing, all mapped reads containing an allelic SNP were counted and the maternal/paternal read ratio was calculated. SNPs containing less than ten reads were excluded from the analysis. For each sample, the ratio across all SNPs for a given gene were averaged. Then, the average and standard error of the mean were calculated for each cell line/condition.

seCLIP-seq, library preparation

15×10^6 $Mirg^{fl/+}$;untag-Ago2 or $Mirg^{fl/+}$;HA-Ago2 ESCs were plated on PEI-coated 15 cm plates and differentiated in N2B27 medium containing 1 ug/mL doxycycline for 10 days (2 biological replicates per cell line). Cells were washed in 1X PBS and then UV cross-linked at 400 mJ/cm2. Immunoprecipitation was performed with 100 uL anti-HA magnetic beads per sample (Pierce) overnight at 4°C. seCLIP-seq libraries were prepared according to (Van Nostrand et al., 2017) with TruSeq LT adapters. Input and IP samples were amplified with 9 and 18 cycles of PCR, respectively. Quality control on final libraries was assessed with a fragment analyzer and qPCR for colony forming units prior to pooling and loading on an Illumina FlowCell (HiSeq2000, 40 bp SE reads). Each sample library was sequenced to a depth of 20-30 M reads.

seCLIP-seq, data analysis pipeline

Adaptor sequences were trimmed from seCLIP-sequencing reads using fastxtoolkit (v0.0.13), followed by removal of PCR duplicated based on unique molecular identifier (UMI), and then the UMI was trimmed with the following commands:

fastx_clipper -a AGATCGGAAGAGCACACGTCTGAACTCCAGTCAC -Q33 -l 15 -v -i $input/ID_sequence.fastq -o $input/ID_sequence_clip.fastq

fastx_collapser -Q33 -v -i $input/ID_sequence_clip.fastq -o $input/ID_sequence_collapse.fastq

fastx_trimmer -f 11 -i $input/ID_sequence_collapse.fastq -o $input/ID_sequence_trim.fastq

To determine which miRNAs were enriched for Ago2 binding, STAR (v2.5.3a) was used to map seCLIP-sequencing reads to mm10 genome (Gencode M15 assembly) with the following command (allowing for reads to map up to 5 locations since some miRNAs are multi-copy in the genome):

STAR–runThreadN 8–runMode alignReads–genomeDir $genome/–readFilesIn $input/ID_sequence_trim.fastq–outFileNamePrefix $input/ID_–outReadsUnmapped Fastx–outFilterMultimapNmax 5–outFilterMultimapScoreRange 1–outSAMtype BAM SortedByCoordinate–outFilterType BySJout–outFilterScoreMin 10–alignEndsType EndToEnd–sjdbGTFfile $genome/gencode.vM15.primary_assembly.annotation.gtf

Biological replicates were merged using samtools. Then for each mature miRNA annotated in miRBase, enrichment for Ago2 binding was calculated in HA-Ago2 IP samples relative to HA-Ago2 Input using seCLIP perl scrips from the Yeo lab (https://github.com/YeoLab/eclip).

To determine which mRNA targets were enriched for Ago2 binding, the same command as above was used but only uniquely mapped reads were considered (by setting–outFilterMultimapNmax = 1). Biological replicates were merged using samtools. Peaks were called on HA-Ago2 IP sample using the CLIPper tool with the following command:

clipper -b $path/HAAgo2IP.merged.bam -s mm10 -o $path/HAAgo2.peaks.bed

Then, enrichment for Ago2 binding at each peak was calculated in HA-Ago2 IP samples relative to HA-Ago2 Input and untag-Ago2 IP using seCLIP perl scrips from the Yeo lab (https://github.com/YeoLab/eclip).

Metagene analysis

Genome (mm10) coordinates for target seed sites of miR-379/410 miRNAs were downloaded from TargetScanMouse (release 7.2). Metagene binding plots were generated from Ago2 seCLIP-seq binding profiles. ".bam" files from merged biological replicates were loaded into the R package metagene (v2.14.0), and coverage (RPM) was calculated at the seed site and the flanking 175-500 nt for all expressed transcripts (expression cutoff = 100 mean normalized counts from RSEM output of RNA-seq analysis). The metagene profile for imprinted genes contains all conserved, predicted seed sites for active miR-379/410 in maternally expressed or paternally expressed protein-coding genes from (Tucci et al., 2019).

Biological network of miR-379/410 targets using Cytoscape

The biological network of gene ontology terms associated with miR-379/410 targets identified from Ago2 seCLIP-seq were analyzed using the Cytoscape (v3.7.1) app, BiNGO. All genes containing significantly enriched Ago2 peaks overlapping a seed site of an active miR-379/410 miRNA were used as the input, and overrepresentation of gene ontology terms was calculated using hypergeometric test and Benjamini & Hochberg FDR correction relative to the reference set of all gene expressed in iNs.

Analysis of *in vivo* Mirg and miR-379/410 expression

microRNA-seq and polyA RNA-seq data from embryonic day 14.5 and postnatal day 0 mouse tissues were downloaded from the ENCODE project (see GSE82864, GSE82558, and GSE78374 for forebrain samples, and related GSE entries for other tissues). Small RNA-seq data from adult mouse tissues were downloaded from GSE21630 (Kuchen et al., 2010). polyA RNA-seq from isolated cortical cell types were downloaded from GSE52564 (Zhang et al., 2014). Raw fastq files from these publicly available datasets were analyzed according to the small RNA-seq and RNA-seq data analysis pipelines described above.

QUANTIFICATION AND STATISTICAL ANALYSIS

For all analysis with p values, significance was determined at $p \leq 0.05$ and values are shown. Hypergeometric statistical test for enrichment was used to calculate the enrichment of miR-379/410 seCLIP targets for paternally expressed genes (N = 13,825 expressed protein-coding genes, n = 63 paternally expressed protein-coding genes, K = 227 miR-379/410 targets from seCLIP-seq, k = 7 miR-379/410 paternally expressed targets). Box-whisker plots were generated using R with the box extending from the 25^{th} to 75^{th} percentile and a thick bar at the 50^{th} percentile. Dashes lines extend from the min to max data points with outliers shown. For CDF analysis, significance was measured using two-sided Kolmogorov-Smirnov (KS) test using the ks.test function in R.

DATA AND CODE AVAILABILITY

Data can be found at GEO with accession GEO: GSE140838. Original gel images were uploaded to Mendeley Data: https://doi.org/10.17632/hf4xvtz8t4.1.

Molecular Cell, Volume *78*

Supplemental Information

Imprinted Maternally Expressed microRNAs Antagonize Paternally Driven Gene Programs in Neurons

Amanda J. Whipple, Vincent Breton-Provencher, Hannah N. Jacobs, Udbhav K. Chitta, Mriganka Sur, and Phillip A. Sharp

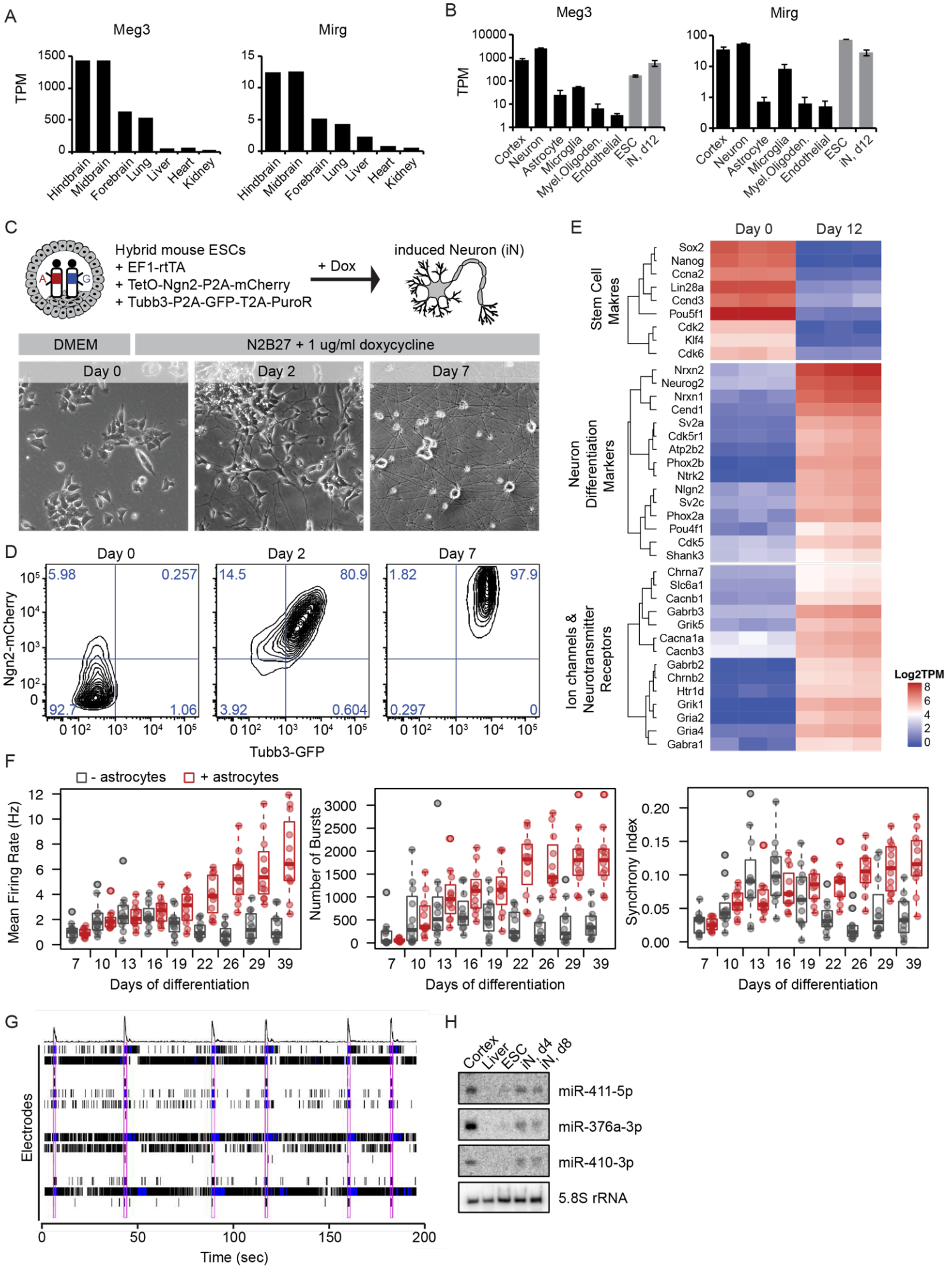
A
Meg3
Mirg
TPM
Hindbrain
Midbrain
Forebrain
Lung
Liver
Heart
Kidney
B
Meg3
Mirg
TPM
Cortex
Neuron
Astrocyte
Microglia
Myel.Oligoden.
Endothelial
ESC
iN, d12
C
Hybrid mouse ESCs
+ EF1-rtTA
+ TetO-Ngn2-P2A-mCherry
+ Tubb3-P2A-GFP-T2A-PuroR
+ Dox
induced Neuron (iN)
DMEM
N2B27 + 1 ug/ml doxycycline
Day 0
Day 2
Day 7
D
Day 0
Day 2
Day 7
Ngn2-mCherry
Tubb3-GFP
5.98
0.257
92.7
1.06
14.5
80.9
3.92
0.604
1.82
97.9
0.297
0
E
Day 0
Day 12
Stem Cell Makres
Sox2
Nanog
Ccna2
Lin28a
Ccnd3
Pou5f1
Cdk2
Klf4
Cdk6
Neuron Differentiation Markers
Nrxn2
Neurog2
Nrxn1
Cend1
Sv2a
Cdk5r1
Atp2b2
Phox2b
Ntrk2
Nlgn2
Sv2c
Phox2a
Pou4f1
Cdk5
Shank3
Ion channels & Neurotransmitter Receptors
Chrna7
Slc6a1
Cacnb1
Gabrb3
Grik5
Cacna1a
Cacnb3
Gabrb2
Chrnb2
Htr1d
Grik1
Gria2
Gria4
Gabra1
Log2TPM
F
- astrocytes
+ astrocytes
Mean Firing Rate (Hz)
Number of Bursts
Synchrony Index
Days of differentiation
G
Electrodes
Time (sec)
H
Cortex
Liver
ESC
iN, d4
iN, d8
miR-411-5p
miR-376a-3p
miR-410-3p
5.8S rRNA

Figure S1. An *in vitro* model system for studying imprinted gene function in neurons, Related to Figure 1

A. Quantification of *Meg3* and *Mirg* expression as transcripts per million (TPM) from postnatal day 0 mouse tissues. **B.** TPM quantification of *Meg3* and *Mirg* expression from cell types isolated from the mouse cortex, in vitro ESCs, and iNs (day 12). Mean ± abs error (n = 2) for neuron, astrocyte, microglia, myelinating oligodendrocyte, and endothelial samples; Mean ± std deviation (n = 3) for whole cortex, ESCs, and iNs. **C.** Schematic overview of Ngn2-induced differentiation and brightfield images of ESCs and iNs (day 2 and 7). **D.** Fluorescence activated cells sorting (FACS) of ESCs and iNs (day 2 and 7) based on Ngn2-mCherry and endogenously tagged Tubb3-GFP. Percentage of cells in each gated quadrant is indicated. **E.** Heatmap of transcripts per million (TPM) from rRNA-depleted RNA-seq of ESCs (day 0, n = 3) and iNs (day 12, n = 3) for stem cell markers, neuron differentiation markers, and ion channels or neurotransmitter receptors. **F.** Analysis of multielectrode array (MEA) recordings for mean firing rate (Hz), number of electrode bursts, and synchrony index across a time course of differentiation. Black, iNs alone; Red, iNs co-cultured with astrocytes. Individual data points are the mean of 16 electrodes in an individual well, and boxplot summarize the data of 12 wells per condition. **G.** An example raster plot of iNs (day 19). The first row is the population histogram and all subsequent rows are tracks of the 16 individual electrodes in the well. Electrode bursts are shown in blue and network bursts are outlined in pink. **H.** Northern blot for three mature miRNAs from miR-379/410 in adult mouse cortex and liver, *in vitro* ESCs, and iNs (day 4 and 8) relative to 5.8S rRNA.

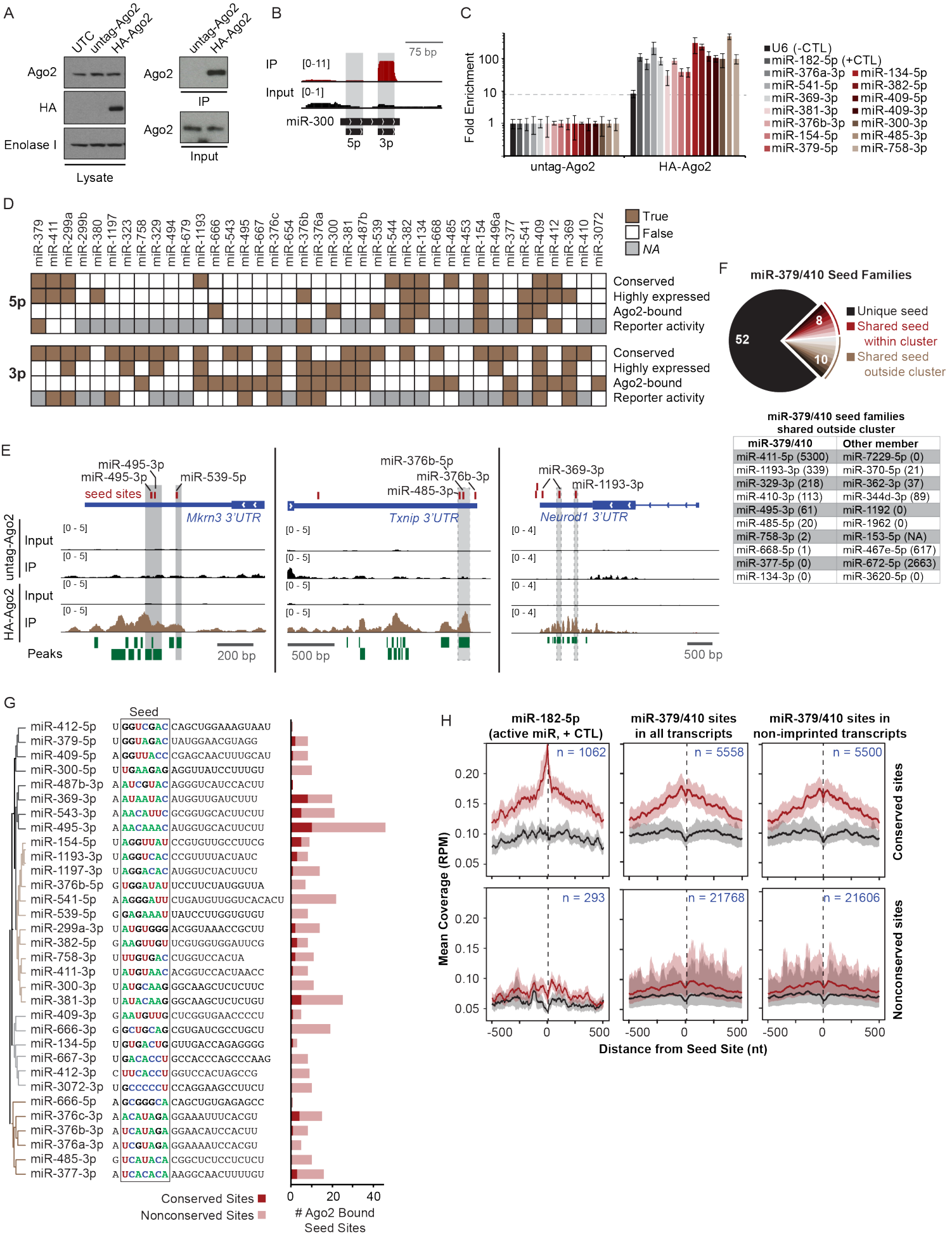

miR-379/410	Other member
miR-411-5p (5300)	miR-7229-5p (0)
miR-1193-3p (339)	miR-370-5p (21)
miR-329-3p (218)	miR-362-3p (37)
miR-410-3p (113)	miR-344d-3p (89)
miR-495-3p (61)	miR-1192 (0)
miR-485-5p (20)	miR-1962 (0)
miR-758-3p (2)	miR-153-5p (NA)
miR-668-5p (1)	miR-467e-5p (617)
miR-377-5p (0)	miR-672-5p (2663)
miR-134-3p (0)	miR-3620-5p (0)

Figure S2. miR-379/410 targeting by Ago2 seCLIP in iNs, Related to Figure 2

A. Western blot from cells with overexpression of untagged-Ago2 or HA-Ago2 from a stably integrated transgene. Left: whole cell lysates probed with antibodies for Ago2, HA, or Enolase I (loading control). UTC, untransfected control with endogenous Ago2 expression. Right: Confirmation of Ago2 immunoprecipitation in seCLIP-seq. Cross-linked cell lysates were immunoprecipitated with an HA antibody. The input and IP samples were then probed with Ago2 antibody. **B.** Genomic alignment of seCLIP-seq reads to miR-300. Scale is reads per million. **C.** RNA immunoprecipitation using an HA antibody for iNs expressing untagged-Ago2 or HA-Ago2 followed by miRNA qRT-PCR. Dotted line indicates enrichment threshold established by U6 snRNA negative control. miR-182-5p is a positive control from outside the miR-379/410 cluster. **D.** Summary of data for each miRNA from miR-379/410 organized according to their 5'-to-3' position within the cluster. Conserved, true if miRNA is conserved among eutherian mammals (from TargetScanMouse, release 7.2); Highly expressed, from Figure 1B; Ago2-bound, from Figure 2A; Reporter activity, from Figure 1G. **E.** Genomic alignment of Ago2 seCLIP-seq reads to the 3' UTR of *Mkrn3, Txnip*, and *Neurod1*. Reads are scaled to reads per million (RPM). Predicted binding sites for active miR-379/410 miRNAs are indicated in red. Significant Ago2 peaks are shown as green boxes. Significant Ago2 peaks overlapping a seed site for miR-379/410 are highlighted in gray. **F.** Top: Pie chart of seed families in miR-379/410 cluster. Unique seed families contain one miR-379/410 miRNA (n = 52, black), seed families with two miR-379/410 family members (n = 8, red), seed families with one miR-379/410 family member and one member outside the cluster (n = 10, gold). Bottom: Table of miR-379/410 seed families that share a seed sequence with a miRNA outside the cluster. Normalized expression counts in iNs for each miRNA are indicated in parenthesis. **G.** Active miR-379/410 miRNAs were clustered according to the similarity of their seed sequence. The mature miRNA sequence is shown and the seed sequence is highlighted. The bar graph indicates the number of significant Ago2 peaks that overlap a conserved or nonconserved seed match for each active miRNA. **H.** Metagene plot of Ago2 seCLIP-seq coverage (reads per million, RPM) at seed sites for the indicated miRNAs, including coverage 500 nt upstream and downstream of the seed site. The number of sites included in each plot is indicated. Top, conserved sites; Bottom, nonconserved sites with TargetScan score ≥ 90; Black, untagged-Ago2 IP; Red, HA-Ago2 IP.

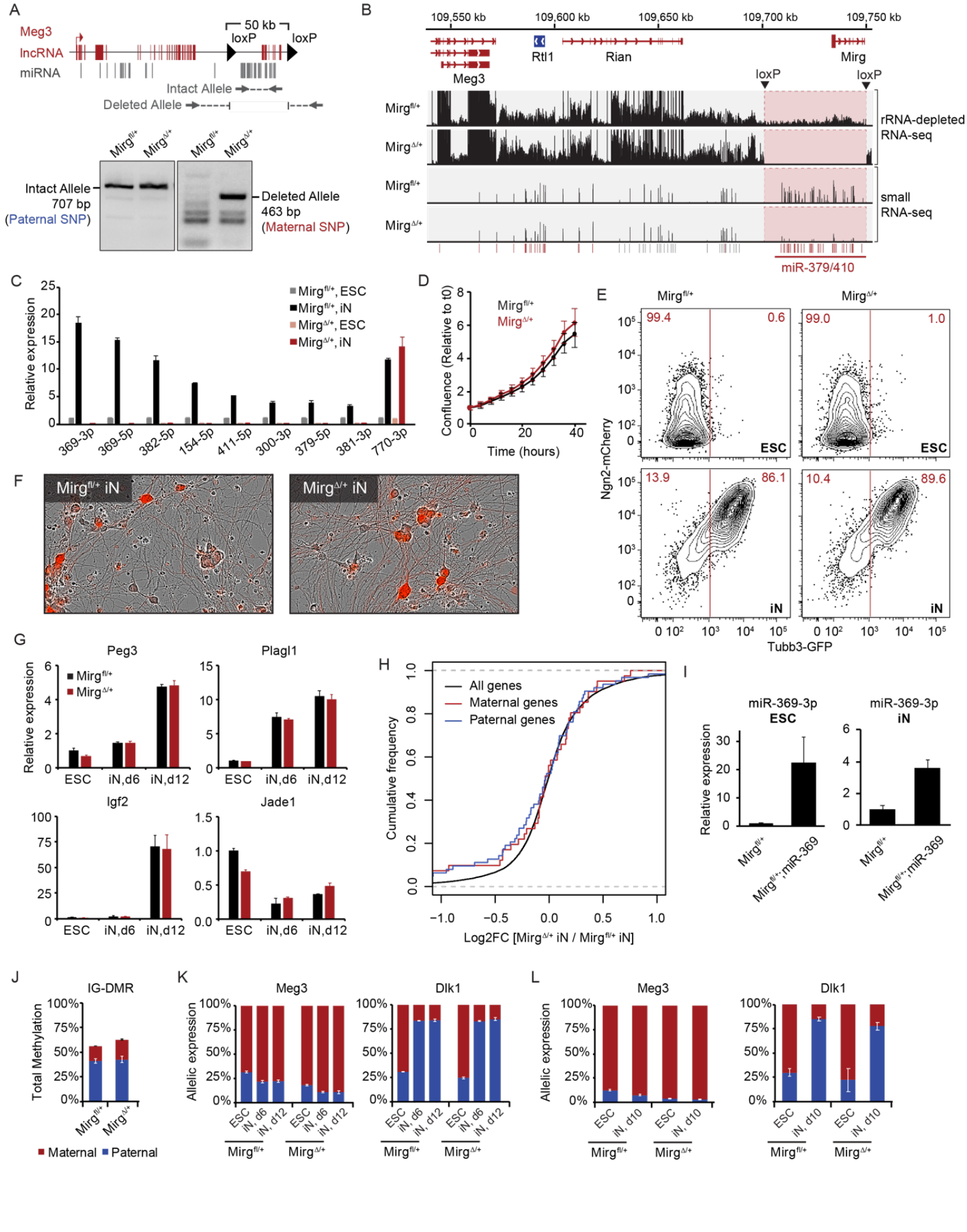
A
Meg3
lncRNA
miRNA
50 kb
loxP
loxP
Intact Allele
Deleted Allele
Mirg^fl/+
Mirg^Δ/+
Intact Allele
707 bp
(Paternal SNP)
Deleted Allele
463 bp
(Maternal SNP)
B
109,550 kb
109,600 kb
109,650 kb
109,700 kb
109,750 kb
Rtl1
Rian
Mirg
Meg3
loxP
loxP
rRNA-depleted RNA-seq
small RNA-seq
miR-379/410
C
Relative expression
Mirg^fl/+, ESC
Mirg^fl/+, iN
Mirg^Δ/+, ESC
Mirg^Δ/+, iN
369-3p
369-5p
382-5p
154-5p
411-5p
300-3p
379-5p
381-3p
770-3p
D
Confluence (Relative to t0)
Time (hours)
E
Mirg^fl/+
Mirg^Δ/+
99.4
0.6
99.0
1.0
13.9
86.1
10.4
89.6
ESC
iN
Ngn2-mCherry
Tubb3-GFP
F
Mirg^fl/+ iN
Mirg^Δ/+ iN
G
Peg3
Plagl1
Igf2
Jade1
Relative expression
ESC
iN,d6
iN,d12
H
All genes
Maternal genes
Paternal genes
Cumulative frequency
Log2FC [Mirg^Δ/+ iN / Mirg^fl/+ iN]
I
miR-369-3p
ESC
miR-369-3p
iN
Relative expression
Mirg^fl/+
Mirg^fl/+;miR-369
J
IG-DMR
Total Methylation
Maternal
Paternal
K
Meg3
Dlk1
Allelic expression
ESC
iN, d6
iN, d12
L
Meg3
Dlk1
Allelic expression
ESC
iN, d10

Figure S3. Characterization of maternal miR-379/410 deletion in ESCs, Related to Figure 3 **A.** Top: Schematic of *Meg3* genomic locus showing location of maternal loxP insertions and primer locations to confirm presence of intact and deleted allele following Cre-mediated recombination. Bottom: Agarose gel of PCR products for intact and deleted allele in $Mirg^{fl/+}$ and $Mirg^{\Delta/+}$ ESCs. Allelic identity was obtained by Sanger sequencing across allelic SNPs from gel isolated bands. **B.** Genomic alignment of rRNA-depleted RNA-seq and small RNA-seq reads to the Chr12 *Meg3* locus in $Mirg^{fl/+}$ and $Mirg^{\Delta/+}$ iNs. **C.** qRT-PCR for mature miRNAs from miR-379/410 in $Mirg^{fl/+}$ and $Mirg^{\Delta/+}$ ESCs and iNs. miR-770-3p is a miRNA transcribed outside the miR-379/410 cluster as an assay control. Mean ± SEM (n = 3). **D.** Proliferation rate was compared between $Mirg^{fl/+}$ and $Mirg^{\Delta/+}$ ESCs by quantifying the confluency of the cell culture dish over time on the Incucyte Imaging System. Mean ± SEM (n = 3). **E.** FACS of ESCs and iNs based on Ngn2-mCherry and endogenously tagged Tubb3-GFP. Percentage of Tubb3-GFP negative or positive cells is indicated. **F.** Overlay of brightfield and Ngn2-mCherry fluorescence images for $Mirg^{fl/+}$ and $Mirg^{\Delta/+}$ iNs. **G.** qRT-PCR for paternally-expressed transcripts in ESCs and iNs (d6, day 6; d12, day 12). **H.** CDF plot of gene expression upon miR-379/410 deletion in iNs for all genes (black, n = 14,325), maternally-expressed genes (red, n = 41, p = 0.9), and paternally-expressed genes (blue, n = 63, p = 0.3). P-values were calculated using two-sided Kolmogorov-Smirnov test. **I.** qRT-PCR for miR-369-3p in $Mirg^{fl/+}$ cells with overexpression of miR-369. **J.** Quantification of allele-specific DNA methylation at the intergenic differentially methylated region (IG-DMR) for the *Dlk1*/*Meg3* locus in $Mirg^{fl/+}$ and $Mirg^{\Delta/+}$ ESCs using pyrosequencing. Mean ± SEM (n = 3). **K.** Allele-specific qRT-PCR for *Meg3* and *Dlk1* expression in $Mirg^{fl/+}$ and $Mirg^{\Delta/+}$ ESCs and iNs. Mean ± SEM (n = 3). **L.** Allele-specific expression of *Meg3* and *Dlk1* by quantification of SNP-containing RNA-sequencing reads in $Mirg^{fl/+}$ and $Mirg^{\Delta/+}$ ESCs and iNs. Mean ± SEM (n = 3).

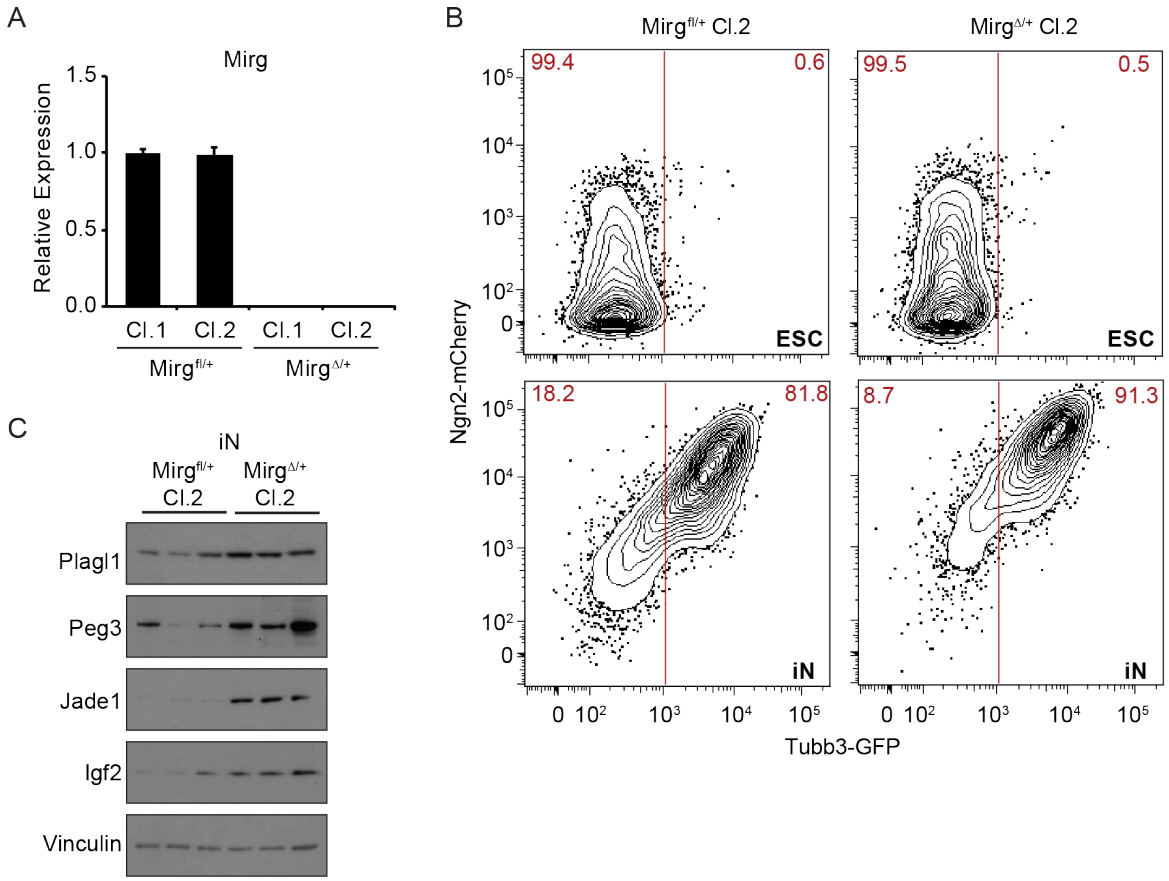

Figure S4. Confirmation of observed changes in a second subclonal Mirg$^{fl/+}$ and Mirg$^{\Delta/+}$ cell line, Related to Figure 3

A. qRT-PCR for *Mirg* in two subclonal cell lines with maternal allele floxed or deleted *Mirg* locus. **B.** FACS of ESCs and iNs based on Ngn2-mCherry and endogenously tagged Tubb3-GFP. Percentage of Tubb3-GFP negative or positive cells is indicated. **C.** Western blot of protein lysates from Mirg$^{fl/+}$ (Clone 2) and Mirg$^{\Delta/+}$ (Clone 2) iNs probed with the indicated antibodies. Vinculin was used as a loading control. Biological triplicates are shown for each condition.

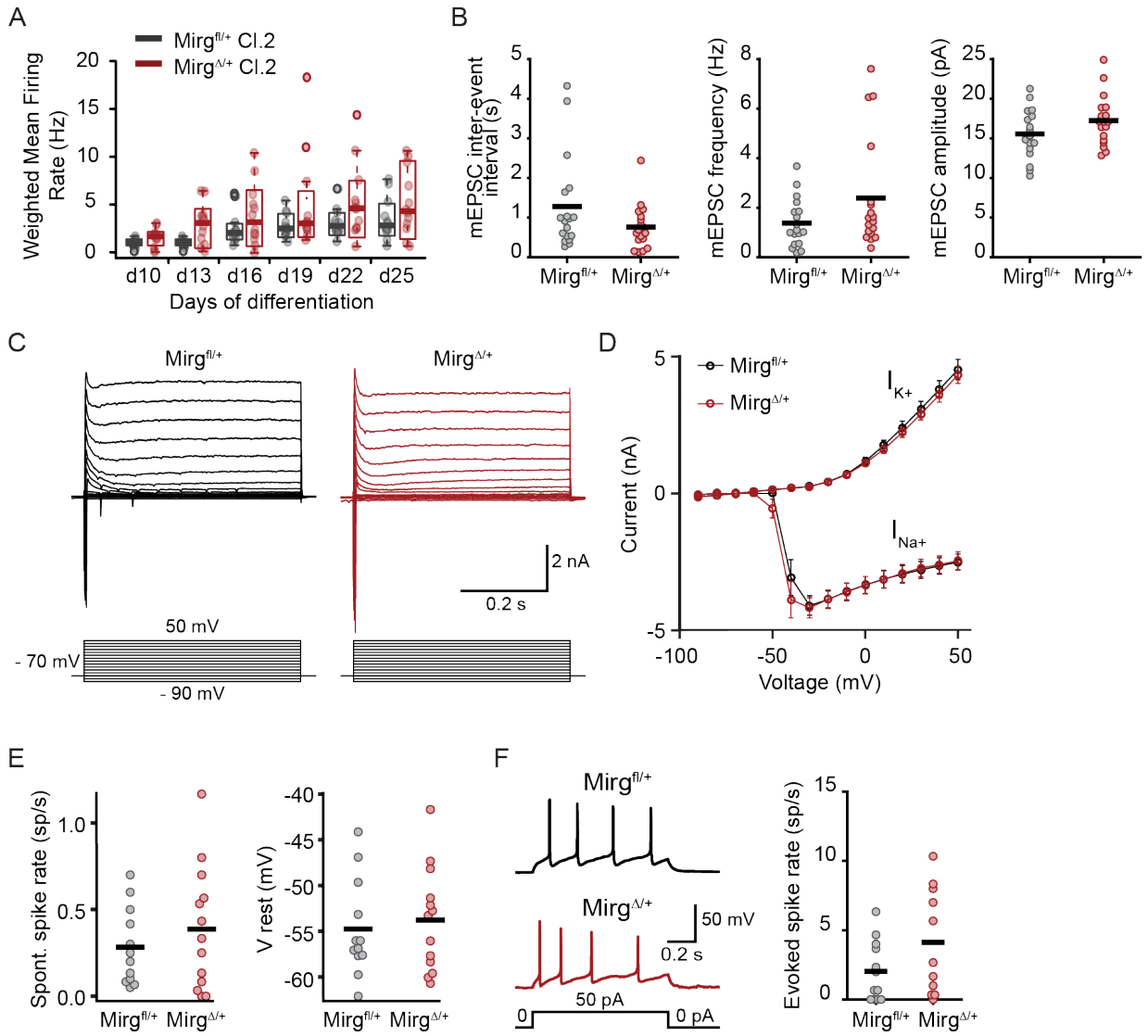

Figure S5. miR-379/410 deletion increases synaptic events but preserves spiking and membrane properties, Related to Figure 5

A. Boxplot of weighted mean firing rate from MEA recordings at day 10 to 25 of differentiation. Individual data points are the mean of 16 electrodes in a single well. Black, $Mirg^{fl/+}$ Clone 2 iNs (n = 12 wells); Red, $Mirg^{\Delta/+}$ Clone 2 iNs (n = 12 wells). **B**. Quantification of inter-event interval (p = 0.10, t_{34} = 1.6773), mEPSC frequency (p = 0.09, t_{34} = -1.7588), and amplitude (p = 0.11, t_{34} = 1.6237) from mEPSC voltage-clamp recordings. Individual data points are the mean values for each cell, n = 18 cells for each condition. Solid black bar represents the mean value for each condition. P-values were calculated using unpaired two-tailed Student's t-test. **C**. Example voltage-clamp trace in response to voltage steps for $Mirg^{fl/+}$ and $Mirg^{\Delta/+}$ iNs. **D**. Amplitude of sodium (I_{Na+}) and potassium (I_{K+}) currents at different voltage steps. Black, $Mirg^{fl/+}$ iNs (n = 12);

Red, $Mirg^{\Delta/+}$ iNs (n = 13); Mean ± SEM. **E**. Spontaneous spike rate ($p = 0.40$, $t_{23} = -0.86$) and resting membrane potential ($p = 0.67$, $t_{23} = -0.44$) measured during one-minute-long current-clamp recordings without current injection. Black, $Mirg^{fl/+}$ iNs (n = 12); Red, $Mirg^{\Delta/+}$ iNs (n = 13). **F**. Left: Representative current-clamp traces of the spiking activity in response to +50 pA current steps for each condition. Right: Average evoked spike rate at 50 pA current injection ($p = 0.12$, $t_{21} = -1.6335$). Black, $Mirg^{fl/+}$ iNs (n = 12); Red, $Mirg^{\Delta/+}$ iNs (n = 11). P-values in (**E**) and (**F**) were calculated using unpaired two-tailed Student's t-test. Solid black bars in (**E**) and (**F**) represent the average value for each condition.